Statistical behaviors of conditioned two-point second-order structure functions in turbulent premixed flames in different combustion regimes

Statistical behaviours of conditioned two-point second-order structure functions in turbulent premixed flames in different combustion regimes

Peter Brearley[1], Umair Ahmed[1], Nilanjan Chakraborty[1*], Andrei Lipatnikov[2]

[1]School of Engineering
Newcastle University
Claremont Road, Newcastle-Upon-Tyne
NE1 7RU, UK

[2]Department of Mechanics and Maritime Sciences
Chalmers University of Technology
Gothenburg, 412 96, Sweden

*Corresponding author
Email: nilanjan.chakraborty@newcastle.ac.uk
Phone No: +44 0191 208 3570
Fax No: +44 0191 208 8600

ABSTRACT

The second-order structure functions and their components conditioned upon various events have been analysed for un-weighted and density-weighted velocities using a Direct Numerical Simulation (DNS) database. The heat release due to combustion has been shown to have significant influences on the structure functions and their components conditioned on different mixture states. The use of density-weighted velocities changes the relative magnitudes of differently conditioned structure functions but does not reduce the scatter of these magnitudes. The structure functions conditioned to constant-density unburned reactants at both points and normalized using the root-mean-square velocity conditioned to the reactants are larger at higher values of mean reaction progress variables $\bar{c}$ (deeper within the flame brush), with this trend being not weakened with increasing turbulence intensity u'/S_L. These results indicate that, contrary to a common belief, combustion-induced thermal expansion can significantly affect the incoming constant-density turbulent flow of unburned reactants even at u'/S_L and Karlovitz number Ka as large as 10 and 18, respectively. The statistical behaviours of the structure functions reveal that the magnitude of the flame normal gradient of the velocity component tangential to the local flames can be significant and it increases with increasing turbulence intensity. Moreover, the structure functions conditioned on both points in the heat release zone bear the signature of the anisotropic effects induced by baroclinic torque for the flames belonging to the wrinkled flamelets and corrugated flamelets regimes. These anisotropic effects weaken with increasing turbulence intensity in the thin reaction zones regime.

Keywords: Structure functions, reactants, products, heat release zone, premixed turbulent flame, Direct Numerical Simulations

I. INTRODUCTION

The structure functions $D_{ij}(\vec{r},\vec{x},t)$, correlation functions $R_{ij}(\vec{r},\vec{x},t)$ and spectra obtained using $R_{ij}(\vec{r},\vec{x},t)$ are of paramount importance in the fundamental understanding of the spatial structure of turbulent flows and have been analysed in detail for non-reacting turbulent flows.[1-4] To date, limited investigations have been directed to the analysis of correlation functions and spectra[5-8] or structure functions[9-11] in turbulent reacting flows. It is well-known that the effects of heat release on turbulent fluid motion significantly modify both the vorticity or/and enstrophy[12-19] and turbulent kinetic energy[20-24] transports in premixed turbulent flames, e.g. through the baroclinic torque and dilatation rate arising from thermal expansion. Furthermore, it has been argued[25-28] and shown both experimentally[29-32] and computationally[12-24] that significant amplification of velocity fluctuations known as flame-generated turbulence[25,28] can occur in flames under certain conditions. There are other manifestations of the heat-release effects [32-34] and interested readers are referred to Refs. 26,35-37 for a detailed review of the existing analyses on the influence of heat release on turbulent flows in flames. The signature of heat release should be reflected in the structure functions, which are widely used for experimental data processing[1-4], fundamental physical understanding[38] and developing models.[39]

To date, only a limited number of investigations[9-11] have focussed on the statistical behaviours of the structure functions in turbulent premixed flames. The analyses by Sabelnikov et al.[9,11] focussed on the two-point velocity correlation statistics in the context of second-order structure functions for weakly turbulent premixed flames in the corrugated flamelets regime[40] where the flame thickness remains smaller than the Kolmogorov length scale. By contrast, Whitman et al.[10] considered a Direct Numerical Simulation (DNS) database of turbulent premixed flames subjected to forced homogeneous isotropic turbulence under high turbulence intensities to analyse the statistical behaviours of structure functions, and to assess their agreements with well-known limiting conditions for non-reacting turbulent flows under both small and large length scale separations.

The effects of heat release are expected to be strong under the conditions analysed by Sabelnikov et al.[9,11], whereas the effects of turbulence are commonly assumed to dominate under high Karlovitz number Ka (i.e. $Ka \gg 1$ where Karlovitz number is the ratio of chemical timescale to small-scale turbulent timescale) conditions investigated by Whitman et al.[10] Thus, the behaviours of the structure function in the flames analysed by Whitman et al.[10] are expected to resemble the corresponding behaviours in the non-reacting turbulence. These analyses address two limiting behaviours in terms of Damköhler number Da (i.e. ratio of large-scale turbulent timescale to chemical timescale) and Karlovitz number Ka. For example, the conditions analysed by Sabelnikov et al.[9,11] deal with the limiting behaviours for $Da \gg 1$ and $Ka \ll 1$, whereas the analysis by Whitman et al.[10] is relevant to $Da < 1$ and $Ka \gg 1$, with the conditioned structure functions being differently defined in these two studies. However, the statistical behaviour of the structure functions in turbulent premixed flames in the intermediate range of Da and Ka (i.e. the largest value of Ka considered in this analysis remains smaller than the smallest value of Karlovitz number considered by Whitman et al.[10], whereas the largest Da considered here remains smaller than the smallest Damköhler number considered by Sabelnikov et al.[9,11]) are yet to be investigated, and the present analysis fills this gap in the existing literature. Moreover, the velocity is affected by thermal expansion as a result of chemical heat release and thus the structure functions based on density-weighted velocities are expected to be different from the corresponding counterparts for the un-weighted velocity components. However, this aspect is yet to be analysed and the current analysis aims to address this void in the existing literature.

In the current analysis, an existing DNS database [41,42] of statistically planar premixed flames subjected to forced isotropic unburned gas turbulence has been considered for a range of different turbulence intensities u'/S_L ,where u' is the root-mean-square turbulent velocity and S_L is the unstretched laminar burning velocity. The velocity vector $\vec{u}$ and density-weighted velocity vector $\vec{u}^* = \rho\vec{u}/\rho_0$ (where ρ is the instantaneous gas density and ρ_0 is the unburned gas density) from the DNS data have been used to analyse the statistical behaviours of the corresponding structure functions in premixed turbulent flames. This density-weighting should not be confused with Favre-averaging operation. The fluid velocity in

premixed flames is affected by thermal expansion as a result of density change and thus density-weighting of velocity (i.e. $\vec{u}^* = \rho\vec{u}/\rho_0$) allows one to understand the flow dynamics without some of the biases (but not all because thermal expansion introduces dilatation rate which also affects the pressure, vorticity and scalar gradient fields in a coupled manner, which cannot be eclipsed by density-weighting of velocity) introduced by thermal expansion effects.

In particular, the current analysis focuses on the following objectives:

1. To analyse the effects of turbulence intensity on the statistical behaviours of the second-order structure functions based on both un-weighted and density-weighted velocities.
2. To indicate the differences between the statistical behaviours of the structure functions based on un-weighted and density-weighted velocities.

The rest of the paper is organised as follows. The mathematical background pertaining to this analysis is provided in Section 2. The numerical implementation and the results with their discussion are provided in Sections 3 and 4, respectively. The final section provides the summary of the main findings and conclusions drawn from this work.

II. MATHEMATICAL BACKGROUND

This paper concentrates only on second-order structure functions based on un-weighted and density-weighted velocity fields. These second-order structure functions are defined as:

$$D_{ij}(\vec{r},t) = \langle [u_i(\vec{x}+\vec{r},t) - u_i(\vec{x},t)][u_j(\vec{x}+\vec{r},t) - u_j(\vec{x},t)] \rangle \quad (1i)$$

$$D^*_{ij}(\vec{r},t) = \langle [u^*_i(\vec{x}+\vec{r},t) - u^*_i(\vec{x},t)][u^*_j(\vec{x}+\vec{r},t) - u^*_j(\vec{x},t)] \rangle \quad (1ii)$$

where $\vec{r}$ is the separation vector with a magnitude of $r = |\vec{r}|$, t is time, $\vec{x}$ and $\vec{x}+\vec{r}$ are the position vectors of two points in question and $\langle \dots \rangle$ refers to an ensemble averaging operation. Equation 1 indicates that $D_{ij}(\vec{r},t)$ and $D^*_{ij}(\vec{r},t)$ signify the second moment of velocity difference associated with eddies of size r. Therefore, $D_{ij}(\vec{r},t)$ and $D^*_{ij}(\vec{r},t)$ are expected to provide the energy content associated with eddies of size r and smaller in physical space **(**instead of considering the wave number space in

the case of the energy spectrum**)** along with several other useful measures. A number of expressions can be obtained from eq. 1 for different flow situations. For example, $D_{ij}(\vec{r},t)$ is expected to be independent of $\vec{x}$ in homogeneous turbulence so one obtains:

$$D_{ij}(\vec{r},t) = 2\langle u_i' u_j' \rangle - R_{ij}(\vec{r},t) - R_{ji}(\vec{r},t) \quad (2)$$

where $u_i' = u_i - \langle u_i \rangle$ is the velocity fluctuation in the i^{th} direction and $R_{ij}(\vec{r},t) = \langle u_i'(\vec{x}+\vec{r},t) u_j'(\vec{x},t) \rangle$ is the correlation function. The correlation function $R_{ij}(\vec{r},t)$ reduces to zero for $r \gg l$, where l is the integral length scale. Thus, for $r \gg l$, one obtains $D_{ij} = 2\langle u_i' u_j' \rangle$ (i.e. $D_{ij} = 2\langle u_i' u_j' \rangle$ for $r \to \infty$) for homogeneous turbulence, which can further be simplified to $D_{ij} = 2u'^2 \delta_{ij}$ for homogeneous isotropic turbulence, where $u' = \sqrt{u_i' u_i'/3}$. Under homogeneous isotropic incompressible flow turbulence, the structure function $D_{ij}(\vec{r},t)$ can be expressed completely in terms of longitudinal structure function $D_{ll}(r,t) = \langle [\vec{u}_l(\vec{x}+\vec{r},t) - \vec{u}_l(\vec{x},t)]^2 \rangle$ as [1-4]

$$D_{ij}(r,t) = D_{nn}(r,t) + [D_{ll}(r,t) - D_{nn}(r,t)] r_i r_j / r^2 \quad (3)$$

where the transverse structure function $D_{nn}(r,t) = \langle [\vec{u}_n(\vec{x}+\vec{r},t) - \vec{u}_n(\vec{x},t)]^2 \rangle$ for isotropic homogeneous incompressible turbulence is given by [1-4]:

$$D_{nn}(r,t) = D_{ll}(r,t) + \frac{\partial D_{ll}(r,t)}{\partial r} \frac{r}{2} \quad (4)$$

In eqs. 3 and 4, $\vec{u}_l = (\vec{u} \cdot \vec{r})\vec{r}/r^2$ is the velocity component in the direction of $\vec{r}$, and $\vec{u}_n = \vec{u} - \vec{u}_l$ is the velocity vector normal to the direction of $\vec{r}$. According to Kolmogorov's theory[38], one obtains $D_{ll}(r,t) = C_L \langle \varepsilon r \rangle^{2/3}$ and $D_{nn}(r,t) = 4D_{ll}(r,t)/3$ for the inertial range, where $C_L = 2.0$ is the universal constant, $\varepsilon = \mu(\partial u_i/\partial x_j)(\partial u_i/\partial x_j)/\rho$ is the dissipation rate of kinetic energy with μ and ρ being dynamic viscosity and density, respectively. Here, the summation convention applies for repeated indexes. For small length scale separation (i.e. $r < \eta$), one obtains: $D_{ij} \propto (\partial u_i/\partial x_k)(\partial u_j/\partial x_l) r_k r_l$, which implies that $D_{nn} = [\rho\langle\varepsilon\rangle/15\mu] r^2$ for homogeneous isotropic turbulence.[4] This behaviour for small separation distance also implies that $D_{ij}(0,t)$ vanishes at the zero-separation distance (i.e. $D_{ij}(0,t) = 0$ for $r \to 0$).

In a homogeneous turbulent flow, $D_{ij}(\vec{r},t) = 2R_{ij}(0,t) - R_{ij}(\vec{r},t) - R_{ij}(-\vec{r},t)$, i.e. the structure functions are directly linked with the correlation functions. In an inhomogeneous turbulent flow, which is more relevant to premixed combustion, the relationship between the structure and correlation functions is not straightforward. Accordingly, the two functions may convey different (complementary) information in such a case. For instance, the correlation (structure) functions appear to be more useful for studying spatial structure of velocity (velocity gradient) field.

In premixed flames, the flow field cannot be considered as either statistically homogeneous or isotropic due to density change and preferential flow acceleration in the local flame normal direction and the assumption of incompressibility is rendered invalid. Thus, the structure functions cannot be readily associated with the correlation functions in premixed turbulent combustion.[9] It is well-known that the velocity magnitude increases from the unburned gas side to the burned gas side of the flame brush in premixed turbulent flames. This type of velocity rise was not accounted for in the turbulence theory by Kolmogorov[38] and thus its applicability for unconditioned turbulence statistics in turbulent premixed flames remains questionable.

Indicator functions play key roles in the statistical analysis of intermittency[43-47] in non-reacting turbulent flows. This concept was adopted by Kuznetsov and Sabelnikov[48] for analysing the influence of intermittency on structure functions, which has been extended for investigating structure function statistics in turbulent premixed flames by Sabelnikov et al.[9,11] The same approach has been adopted in the present analysis.

Here, the flames are taken to be statistically planar and stationary, and the mean direction of propagation is aligned in the x_1-direction (right to left). This suggests that velocity is statistically homogeneous in $x_2 - x_3$ planes at a given x_1-location. Thus, the analysis of the structure function statistics will be limited to two points $\vec{x}_A = \{x_{AB}, y_A, z_A\}$ and $\vec{x}_B = \{x_{AB}, y_A + r_y, z_A + r_z\}$ and these points are located at the same transverse plane $x_1 = x_{AB}$ with $\vec{r} = \{0, r_y, r_z\}$ being the distance vector. Indictor functions

$I_\alpha(\vec{x},t)$ at point $\vec{x}_A$ and $I_\beta(\vec{x},t)$ at point $\vec{x}_B$ for $\alpha,\beta = r,p,f$ have been considered in the following manner. The indicator function $I_r(\vec{x},t) = 1.0$ in the constant-density unburned reactants and elsewhere it vanishes. By contrast, the indicator function $I_p(\vec{x},t) = 1.0$ in the constant-density products and it vanishes elsewhere, whereas $I_f(\vec{x},t) = 1.0$ within the flame and vanishes in both the reactants and products. Thus, one obtains the following identity $I_r(\vec{x},t) + I_p(\vec{x},t) + I_f(\vec{x},t) = 1.0$. This leads to the following expression for a general quantity $Q(\vec{x},t)$ [9,11]

$$\langle Q(\vec{x},t)\rangle = \langle Q(\vec{x},t)\sum_\alpha I_\alpha(\vec{x},t)\rangle = \langle\sum_\alpha Q(\vec{x},t)I_\alpha(\vec{x},t)\rangle = \sum_\alpha\langle Q(\vec{x},t)I_\alpha(\vec{x},t)\rangle = \sum_\alpha Q_\alpha(x_1,t)\ P_\alpha(x_1,t) \quad (5)$$

where $Q_\alpha(x_1,t) = \langle Q(\vec{x},t)I_\alpha(\vec{x},t)\rangle/P_\alpha(x_1,t)$ is the value of $Q(\vec{x},t)$ conditioned on state α and $P_\alpha(x_1,t) = \langle I_\alpha(\vec{x},t)\rangle$ is the probability of finding state α in transverse plane x_1 =const.

Based on this formulation, the quantity $(u_{B,i} - u_{A,i})(u_{B,j} - u_{A,j})$ for $\vec{x}_A = \{x_{AB}, y_A, z_A\}$ and $\vec{x}_B = \{x_{AB}, y_A + r_y, z_A + r_z\}$ can be written as[9,11]:

$$\big(u_{B,i} - u_{A,i}\big)\big(u_{B,j} - u_{A,j}\big) = \big(u_{B,i} - u_{A,i}\big)\big(u_{B,j} - u_{A,j}\big)\sum_{\alpha=1}^{3} I_\alpha\,(\vec{\boldsymbol{x}}_{\boldsymbol{A}}, t)\sum_{\beta=1}^{3} I_\beta\,(\vec{\boldsymbol{x}}_{\boldsymbol{B}}, t) \quad (6)$$

where subscripts i,j are applicable for the spatial directions, whereas subscripts α,β refer to the state of the mixture. On averaging eq. 6 over the transverse plane (which is considered to be statistically homogeneous) one gets [9,11]:

$$D_{ij}(x_1,r,t) = \sum_{\alpha=1}^{3}\sum_{\beta=1}^{3} D_{ij}^{\alpha\beta}\,(x_1,r,t)P_{\alpha\beta}(x_1,t) \quad (7)$$

where $D_{ij}^{\alpha\beta}(x_1,r,t)$ is the conditioned structure function, which is given by:

$$D_{ij}^{\alpha\beta}(x_1,r,t) = \langle\big(u_{B,i} - u_{A,i}\big)\big(u_{B,j} - u_{A,j}\big)I_\alpha I_\beta\rangle/P_{\alpha\beta}. \quad (8)$$

Here, $P_{\alpha\beta} = \langle I_\alpha I_\beta\rangle$ is the probability of finding mixture states α and β at points $\vec{x}_A$ and $\vec{x}_B$ respectively that belong to the same transverse plane $x_1 = x_{AB}$ and are separated by distance r. The probability is averaged over that transverse plane. Using r,p,f for mixture conditions referring to unburned reactants, products and reacting mixtures, it is possible to obtain six different conditioned structure functions (i.e. $D_{ij}^{rr}, D_{ij}^{rp}, D_{ij}^{rf}, D_{ij}^{rr}, D_{ij}^{pp}$ and D_{ij}^{ff}) and six different probabilities (i.e. $P_{rr}, P_{rp}, P_{rf}, P_{pp}, P_{fp}$ and P_{ff}). Here rr, rp, rf, pp, pf and ff refer to the following states:

$rr =$ both points are in the reactants

$rp = pr =$ one point is in the reactants and the other is in the products

$rf = fr =$ one point is in the reactants and the other is in the reacting mixture

$pp =$ both points are in the products

$fp = pf =$ one point is in the products and the other is in the reacting mixture

$ff =$ both points are in the reacting mixture.

It is worth noting that the order of the indices α and β is irrelevant to the analysis carried out in this paper and thus $rp = pr, rf = fr$ and $fp = pf$ have been considered. Expressions similar to eqs. 7 and 8 can be derived for the structure functions based on density-weighted velocities (i.e. $D_{ij}^{rr*}, D_{ij}^{rp*}, D_{ij}^{rf*}, D_{ij}^{pp*}, D_{ij}^{fp*}$ and D_{ij}^{ff*}). These structure functions (i.e. $D_{ij}^{rr}, D_{ij}^{rp}, D_{ij}^{rf}, D_{ij}^{pp}, D_{ij}^{fp}, D_{ij}^{ff}$ and $D_{ij}^{rr*}, D_{ij}^{rp*}, D_{ij}^{rf*}, D_{ij}^{pp*}, D_{ij}^{fp*}, D_{ij}^{ff*}$) alongside the corresponding probabilities (i.e. $P_{rr}, P_{rp}, P_{rf}, P_{pp}, P_{pf}$ and P_{ff}) for statistically planar premixed flames for different turbulence intensities will be discussed in Section 4 of this paper.

III. NUMERICAL IMPLEMENTATION

A DNS database[41,42] of statistically planar turbulent premixed flames has been considered for this analysis. The simulations were carried out using a well-known DNS code SENGA+[49] where the conservation equations of mass, momentum, energy and species are solved in non-dimensional form. A single step Arrhenius type irreversible chemical reaction is taken to represent the chemical mechanism for the purpose of computational economy. As the current analysis concentrates on turbulent velocity statistics, the simplification in terms of chemical mechanism is not expected to substantially influence the results presented here. It has been demonstrated in the past that displacement speed statistics from simple chemistry [50-52] and detailed chemistry[53-55] DNS are qualitatively similar. The same is true for the statistics of the reactive scalar gradient obtained from simple chemistry[56-58] and detailed chemistry[58,59] DNS studies. Moreover, the vorticity and sub-grid flux statistics obtained from simple chemistry[14,60] DNS are found to be qualitatively consistent with those obtained from detailed chemistry DNS.[17,61] Furthermore, it has previously been shown that several models developed based on simple

chemistry data[60,62] have been found to perform equally well in the context of detailed chemistry and transport.[61,63] The reaction progress variable c in the context of single step chemistry can be uniquely defined in terms of the reactant mass fraction Y_r as: $c = (Y_{r0} - Y_r)/(Y_{r0} - Y_{r\infty})$ where the subscripts 0 and ∞ indicate values in the unburned gas and fully burned products, respectively.

All the spatial derivatives for the internal grid points have been evaluated using a 10th order central difference scheme and the order of differentiation gradually decreases to a 2nd order one-sided scheme at the non-periodic boundaries in the numerical framework of SENGA+.[49] A 3rd order explicit Runge-Kutta scheme has been used for explicit time-advancement.[64] The present simulations have been conducted in an inlet-outlet configuration where the inlet and outlet boundaries are taken in the direction of mean flame propagation, whereas the transverse boundaries have been considered to be periodic. The boundary conditions have been specified according to the Navier-Stokes Characteristic Boundary Conditions (NSCBC) technique.[65] The outflow boundary is taken to be partially non-reflecting and the mean inlet velocity U_{mean} has been gradually modified to match the turbulent flame speed so that the flame remains within the computational domain.

The simulation domain, the size of the uniform Cartesian grid used for discretising the domain along with the inlet values of root-mean-square turbulent velocity fluctuation normalised by the unstretched laminar burning velocity u'/S_L, integral length scale to thermal flame thickness ratio l/δ_{th}, Damköhler number $Da = lS_L/u'\delta_{th}$, Karlovitz number $Ka = (u'/S_L)^{3/2}(l/\delta_{th})^{-1/2}$ and heat release parameter $\tau = (T_{ad} - T_0)/T_0$ are provided in Table 1 along with the domain and grid sizes, where $\delta_{th} = (T_{ad} - T_0)/\max|\nabla T|_L$ is the thermal flame thickness with T, T_0 and T_{ad} being the dimensional temperature, unburned gas temperature and the adiabatic flame temperature, respectively. The Cartesian grid used for this analysis ensures at least 10 grid points within δ_{th} and 1.5 grid points within the Kolmogorov length scale η. The Lewis number (i.e. $Le = \lambda/\rho C_p D = 1.0$) is taken to be unity for all species and the gases are considered to obey the ideal gas law where λ, C_p and D are the thermal conductivity, specific heat at constant pressure and reaction progress variable diffusivity, respectively. Standard values are

considered for Prandtl number (i.e. $Pr = \mu C_p/\lambda = 0.7$ with μ being the dynamic viscosity), Zel'dovich number (i.e. $\beta = T_{ac}(T_{ad} - T_0)/T_{ad}^2 = 6.0$ with T_{ac} being the activation temperature) and the ratio of specific heats (i.e. $\gamma = C_p/C_v = 1.4$, where C_v is the specific heat at constant volume). The cases considered here span from the wrinkled flamelet regime to the thin reaction zones regime.[40]

Cases	u'/S_L	l/δ_{th}	Da	Ka	τ	Domain	Grid	Regime
A	1.0	3.0	3.0	0.58	4.5	$79.5\delta_{th} \times (39.8\delta_{th})^2$	$800 \times 400 \times 400$	Wrinkled/Corrugated flamelets
B	2.5	3.0	1.2	2.28	4.5	$79.5\delta_{th} \times (39.8\delta_{th})^2$	$800 \times 400 \times 400$	Corrugated flamelets
C	3.0	3.0	1.0	3.0	4.5	$79.5\delta_{th} \times (39.8\delta_{th})^2$	$800 \times 400 \times 400$	Thin reaction zones
D	5.0	3.0	0.6	6.5	4.5	$79.5\delta_{th} \times (39.8\delta_{th})^2$	$800 \times 400 \times 400$	Thin reaction zones
E	7.5	3.0	0.4	11.9	4.5	$79.5\delta_{th} \times (39.8\delta_{th})^2$	$800 \times 400 \times 400$	Thin reaction zones
F	10.0	3.0	0.3	18.3	4.5	$79.5\delta_{th} \times (39.8\delta_{th})^2$	$800 \times 400 \times 400$	Thin reaction zones

Table 1: The attributes of the DNS database considered for this analysis.

A recently proposed modified bandwidth filtered forcing method in the physical space [66] has been used where the forcing term remains proportional to $(1 - c)$ and thus the contribution of the forcing decays across the flame. This forcing method not only maintains the prescribed turbulence intensity u'/S_L but also provides the required integral length scale to flame thickness ratio l/δ_{th}. In the current configuration there is no inherent mechanism to maintain turbulence and without forcing turbulence decays with time. Under decaying turbulence each case will be at different stages of evolution and the integral length scales will be at different values. This will also be true if turbulence is injected through inlet because turbulence evolves differently before it interacts with the flame depending on the flame brush thickness and even may give rise to some instabilities.[66] Thus, it would have been difficult to compare the structure function statistics between different cases under decaying turbulence. In order to avoid this difficulty, the forcing is used for the unburned gas but it is gradually switched off within the flame so that turbulence can evolve within the flame without any influence of forcing. There have been several previous DNS analyses on premixed turbulent combustion[10,67-69] where forcing was used. The merits and demerits of DNS with and without forcing have been discussed in Ref. 66 in detail.

All the simulations listed in Table 1 have been continued until the turbulent kinetic energy and integral length scale attain the desired values and also the turbulent flame speed S_T and flame surface area A_T settle to statistically stationary values. This duration remains greater than the throughpass time (i.e. $t_{sim} > L_x/U_{mean}$) and at least 10 eddy turn over times (i.e. $t_{sim} > 10l/u'$) for all cases. The contours and isosurfaces of c for the cases considered here have been provided elsewhere[41,42] and thus will not be repeated in this analysis.

The Reynolds-averaged/Favre-averaged quantities are extracted by averaging in time and in the homogeneous directions (i.e. x_2 and x_3 directions), which are the transverse directions normal to the mean flame propagation direction in the current configuration. In statistically planar flames the Reynolds-averaged/Favre-averaged reaction progress variable remains a unique function of the coordinate in the direction of mean flame propagation (i.e. x_1-direction). Accordingly, all results will be presented as a function of the Reynolds-averaged reaction progress variable $\bar{c}$ in the following.

The quantities conditioned on reactants and products are evaluated based on $c(\vec{x},t) < \epsilon$ and $c(\vec{x},t) > (1-\epsilon)$, respectively, where ϵ is a predetermined small number. An alteration of ϵ from 0.01 to 0.05 did not modify the results. Thus, the analysis has been carried out for $\epsilon = 0.05$. This ensures $I_r = 1.0$ for $c \leq 0.05$ and 0.0 elsewhere. Similarly $I_p = 1.0$ for $0.95 \leq c \leq 1.0$ and vanishes elsewhere. By contrast, $I_f = 1.0$ for $0.05 < c < 0.95$ and vanishes elsewhere.

In the following, the adjectives 'longitudinal' and 'transverse' for the structure functions will be used only with respect to the direction of Cartesian co-ordinates. It is worthwhile to recognise that the structure functions for premixed flames could be constructed in various different manner (e.g. Whitman et al.[10] considered flame normal and tangential directions) with each methodology offering different insights. A comparison of different approaches is beyond the scope of this analysis and the present analysis will follow the approach outlined by Sabelnikov et al.[9,11] In this framework, the transverse

structure functions $D_{11,T}(r)$ and $D^*_{11,T}(r)$ and their conditioned components are evaluated by (conditionally) averaging $\left(u_{B,1}-u_{A,1}\right)^2$ and $\left(u^*_{B,1}-u^*_{A,1}\right)^2$ for two set of points given by $\vec{x}_A=\{x,y,z\}$; $\vec{x}_B=\{x,y+r,z\}$ and by $\vec{x}_A=\{x,y,z\}$; $\vec{x}_B=\{x,y,z+r\}$. The transverse structure functions $D_{22,T}(r)$ and $D_{33,T}(r)$ (or $D^*_{22,T}(r)$ and $D^*_{33,T}(r)$) are evaluated by averaging $\left(u_{B,2}-u_{A,2}\right)^2$ and $\left(u_{B',3}-u_{A',3}\right)^2$ (or $\left(u^*_{B,2}-u^*_{A,2}\right)^2$ and $\left(u^*_{B',3}-u^*_{A',3}\right)^2$) respectively based on points $\vec{x}_A=\{x,y,z\}$; $\vec{x}_B=\{x,y,z+r\}$ and $\vec{x}_{A'}=\{x,y,z\}$; $\vec{x}_{B'}=\{x,y+r,z\}$, respectively. Finally, the longitudinal transverse structure functions $D_{22,L}(r)$ and $D_{33,L}(r)$ (or $D^*_{22,L}(r)$ and $D^*_{33,L}(r)$) are evaluated by averaging $\left(u_{B,2}-u_{A,2}\right)^2$ and $\left(u_{B',3}-u_{A',3}\right)^2$ (or $\left(u^*_{B,2}-u^*_{A,2}\right)^2$ and $\left(u^*_{B',3}-u^*_{A',3}\right)^2$) respectively based on points $\vec{x}_A=\{x,y,z\}$; $\vec{x}_B=\{x,y+r,z\}$ and $\vec{x}_{A'}=\{x,y,z\}$; $\vec{x}_{B'}=\{x,y,z+r\}$. In the present analysis, $D_{23,T}(r)=0.5[D_{22,T}(r)+D_{33,T}(r)]$ and $D_{23,L}(r)=0.5[D_{22,L}(r)+D_{33,L}(r)]$ (or $D^*_{23,T}(r)=0.5[D^*_{22,T}(r)+D^*_{33,T}(r)]$ and $D^*_{23,L}(r)=0.5[D^*_{22,L}(r)+D^*_{33,L}(r)]$) have been evaluated to account for the possible slight departure from isotropy in the homogeneous directions.

IV. RESULTS & DISCUSSION

The normalised conditioned structure functions $D^{\alpha\beta}_{11,T}(r)/(\tau S_L)^2$ and $D^{\alpha\beta*}_{11,T}(r)/(\tau S_L)^2$ as a function of r/δ_{th} at $\bar{c}=0.5$ are shown in Fig. 1 for cases A-F. The corresponding variations of $D^{\alpha\beta}_{23,T}(r)/(\tau S_L)^2$ and $D^{\alpha\beta*}_{23,T}(r)/(\tau S_L)^2$ (or $D^{\alpha\beta}_{23,L}(r)/(\tau S_L)^2$ and $D^{\alpha\beta*}_{23,L}(r)/(\tau S_L)^2$) are shown in Fig. 2 (or Fig. 3). The unconditioned structure functions $D_{11,T}$, $D_{23,T}$, $D_{23,L}$, $D^*_{11,T}$, $D^*_{23,T}$, $D^*_{23,L}$ are shown as black dotted lines in Figs. 1-3. It is worth noting that the velocity jump across the steady laminar premixed flame is given by τS_L and thus the structure functions are normalised by this quantity as it does not change from one case to another for the database considered here. This will also allow for the quantitative comparison of the magnitudes of the structure functions for the different cases considered here. It is important to recognise that the velocity scale τS_L is merely used for normalising the structure functions and by doing that it is not implied that the structure functions scale with $(\tau S_L)^2$. The choice of $\bar{c}=0.5$ is driven by the fact that the probabilities of finding reactants and products are likely to be significant. Therefore, the probabilities $P_{\alpha\beta}$ are likely to be significant for all conditioned components for this $\bar{c}$, which can be

substantiated from Fig. 4. The results presented in this paper remain qualitatively similar for other $\bar{c}$ values unless it is mentioned otherwise. The probabilities P_{rr}, P_{pp} and P_{ff} decrease with increasing r, whereas the probabilities P_{rf}, P_{rp} and P_{fp} increase with an increase in r before becoming insensitive to the changes in r. The probability of finding identical states of the gaseous mixture is expected to be sufficiently large for small separation distances, whereas these states are likely to be different when the separation distance increases, which explains the observed variations of $P_{\alpha\beta}$ in Fig. 4.

Case	$\frac{\max(D_{11,T})}{2\langle u'_1 u'_1\rangle}$	$\frac{\max(D_{23,T})}{\langle u'_2 u'_2\rangle + \langle u'_3 u'_3\rangle}$	$\frac{\max(D_{23,L})}{\langle u'_2 u'_2\rangle + \langle u'_3 u'_3\rangle}$
A	1.053	1.169	1.136
B	1.415	0.972	1.004
C	1.151	0.997	1.122
D	0.800	1.136	1.120
E	1.156	1.036	1.000
F	0.851	0.968	0.929

Table 2. Values of $\max(D_{11,T})/2\langle u'_1 u'_1\rangle$, $\max(D_{23,T})/\{\langle u'_2 u'_2\rangle + \langle u'_3 u'_3\rangle\}$, $\max(D_{23,L})/\{\langle u'_2 u'_2\rangle + \langle u'_3 u'_3\rangle\}$ for $\bar{c} = 0.5$.

It is clear from Figs. 1-3 that there are significant differences between all the conditioned and unconditioned mean structure functions for all cases considered here, which imply that the heat release due to combustion and reactant-product intermittency play significant roles in the turbulent flow structure in premixed turbulent flames. A comparison of the left and right columns of Figs. 1, 2, or 3 shows that the use of the density-weighted structure functions is not sufficient to eliminate significant differences between differently conditioned structure functions. The maximum values of the normalised structure functions $D_{11,T}^{\alpha\beta}(r)/(\tau S_L)^2$, $D_{23,T}^{\alpha\beta}(r)/(\tau S_L)^2$ and $D_{23,L}^{\alpha\beta}(r)/(\tau S_L)^2$ (or $D_{11,T}^{\alpha\beta*}(r)/(\tau S_L)^2$, $D_{23,T}^{\alpha\beta*}(r)/(\tau S_L)^2$ and $D_{23,L}^{\alpha\beta*}(r)/(\tau S_L)^2$) increase with increasing turbulence intensity (i.e. from case A to case F). As turbulence is not homogeneous within the flame brush (e.g. at $\bar{c} = 0.5$ location), it cannot be expected that the maximum value of the unconditioned structure function D_{ij} is going to same as that of $2\langle u_i' u_j'\rangle$ within the flame brush. However, it can be seen from Table 2 that $\max(D_{11,T})/2\langle u'_1 u'_1\rangle$, $\max(D_{23,T})/\{\langle u'_2 u'_2\rangle + \langle u'_3 u'_3\rangle\}$ and $\max(D_{23,L})/\{\langle u'_2 u'_2\rangle + \langle u'_3 u'_3\rangle\}$

remain of the order of unity at $\bar{c} = 0.5$ for all cases considered here. A similar result is obtained for other values of $\bar{c}$.

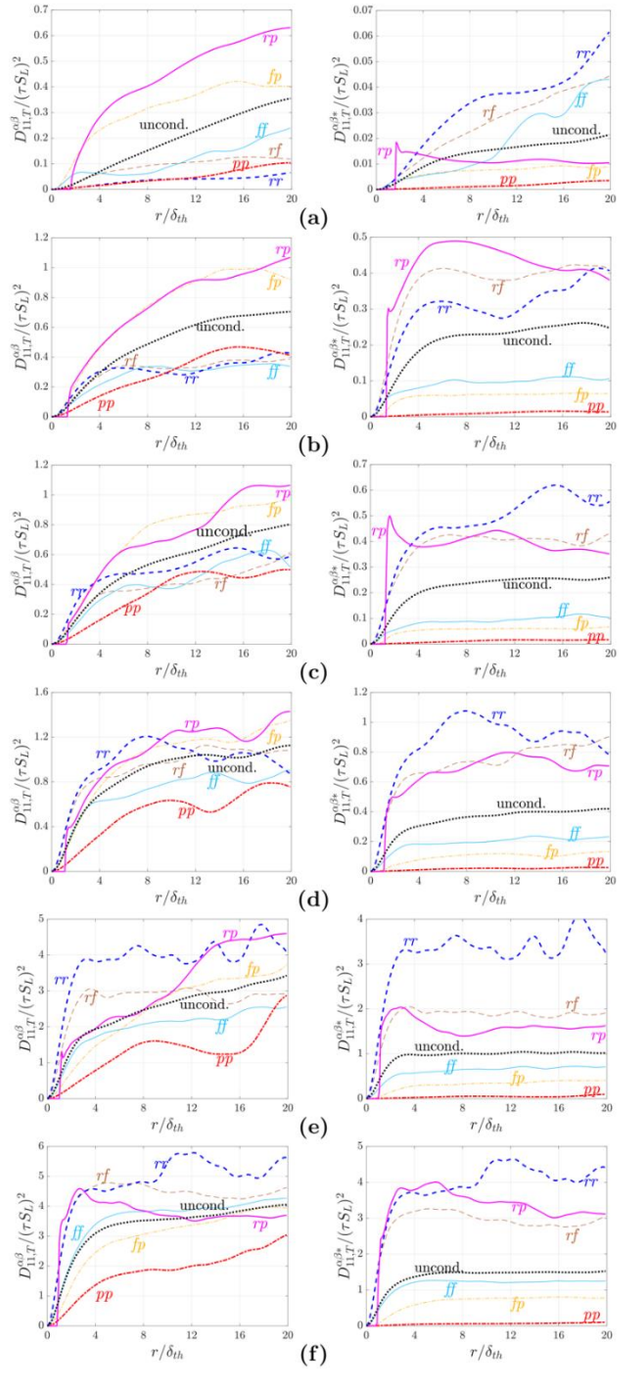

Fig. 1: Variations of normalised transverse conditioned structure functions (coloured lines) $D^{\alpha\beta}_{11,T}(r)/(\tau S_L)^2$ (left column) and $D^{\alpha\beta*}_{11,T}(r)/(\tau S_L)^2$ (right column) and mean unconditioned structure functions (black dots) $D_{11,T}(r)/(\tau S_L)^2$ (left column) and $D^{*}_{11,T}(r)/(\tau S_L)^2$ (right column) for axial velocities as a function of normalised separation distance r/δ_{th} for (a-f) cases A-F at $\bar{c} = 0.5$. Here, $D^{\alpha\beta*}_{11,T}(r)/(\tau S_L)^2$ and $D^{*}_{11,T}(r)/(\tau S_L)^2$ are normalised structure functions based on the density-weighted velocity $\vec{u}^* = \rho\vec{u}/\rho_0$.

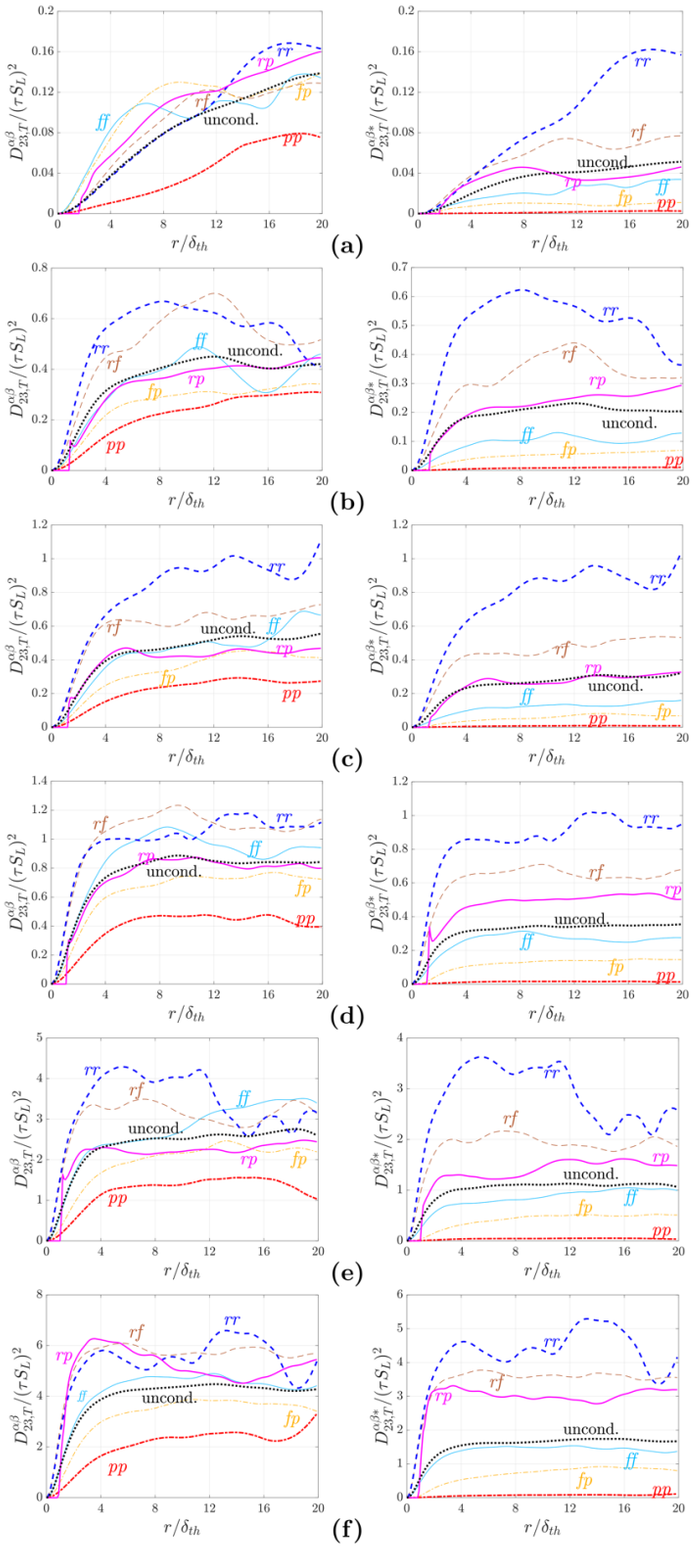

Fig. 2: Variations of normalised transverse conditioned structure functions (coloured lines) $D^{\alpha\beta}_{23,T}(r)/(\tau S_L)^2$ (left column) and $D^{\alpha\beta*}_{23,T}(r)/(\tau S_L)^2$ (right column) and mean unconditioned structure functions (black dots) $D_{23,T}(r)/(\tau S_L)^2$ (left column) and $D^{*}_{23,T}(r)/(\tau S_L)^2$ (right column) for transverse velocities as a function of normalised separation distance r/δ_{th} for (a-f) cases A-F at $\bar{c} = 0.5$. Here, $D^{\alpha\beta*}_{23,T}(r)/(\tau S_L)^2$ and $D^{*}_{23,T}(r)/(\tau S_L)^2$ are normalised structure functions based on the density-weighted velocity $\vec{u}^* = \rho\vec{u}/\rho_0$.

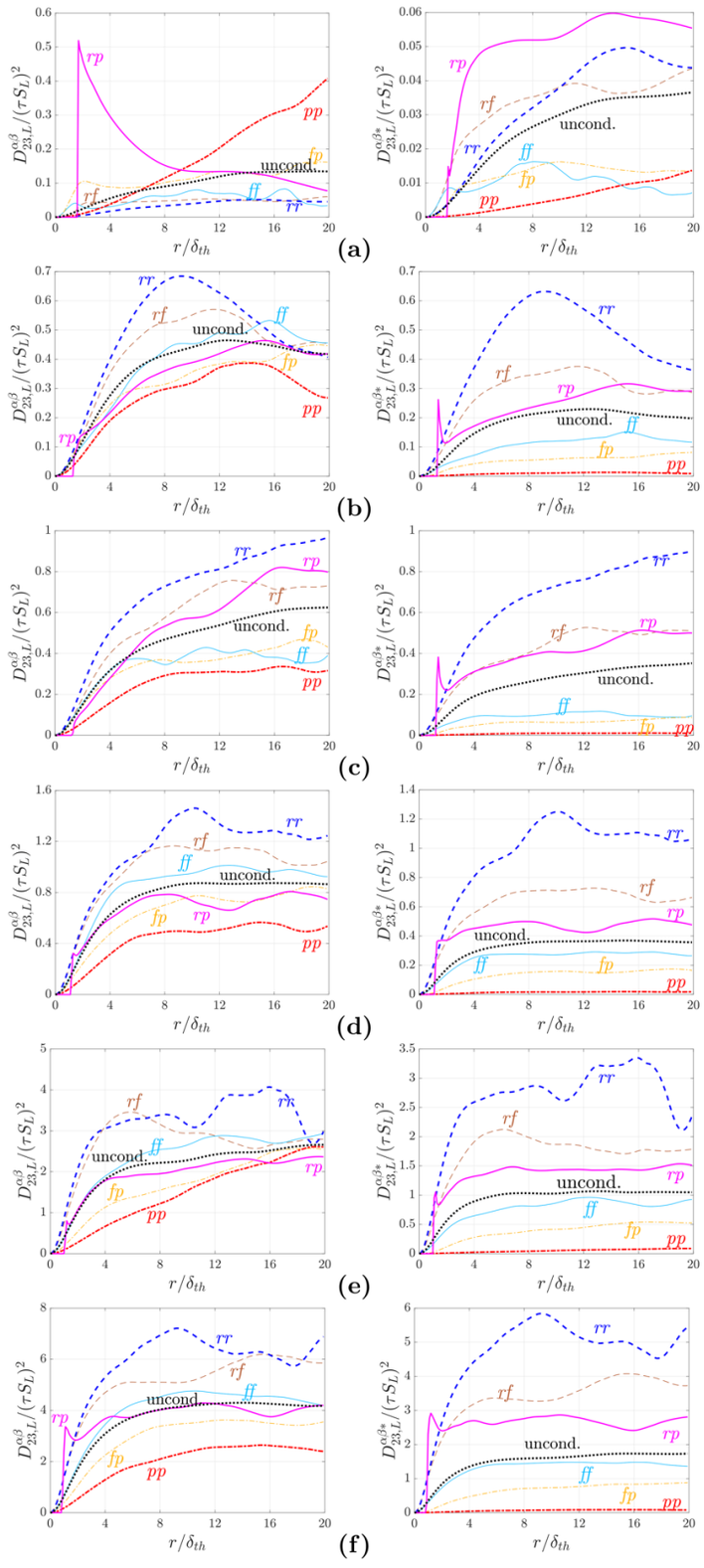

Fig. 3: Variations of normalised longitudinal conditioned structure functions (coloured lines) $D^{\alpha\beta}_{23,L}(r)/(\tau S_L)^2$ (left column) and $D^{\alpha\beta*}_{23,L}(r)/(\tau S_L)^2$ (right column) and mean unconditioned structure functions (black dots) $D_{23,L}(r)/(\tau S_L)^2$ (left column) and $D^{*}_{23,L}(r)/(\tau S_L)^2$ (right column) for transverse velocities as a function of normalised separation distance r/δ_{th} for (a-f) cases A-F at $\bar{c} = 0.5$. Here, $D^{\alpha\beta*}_{23,L}(r)/(\tau S_L)^2$ and $D^{*}_{23,L}(r)/(\tau S_L)^2$ are normalised structure functions based on the density-weighted velocity $\vec{u}^* = \rho\vec{u}/\rho_0$.

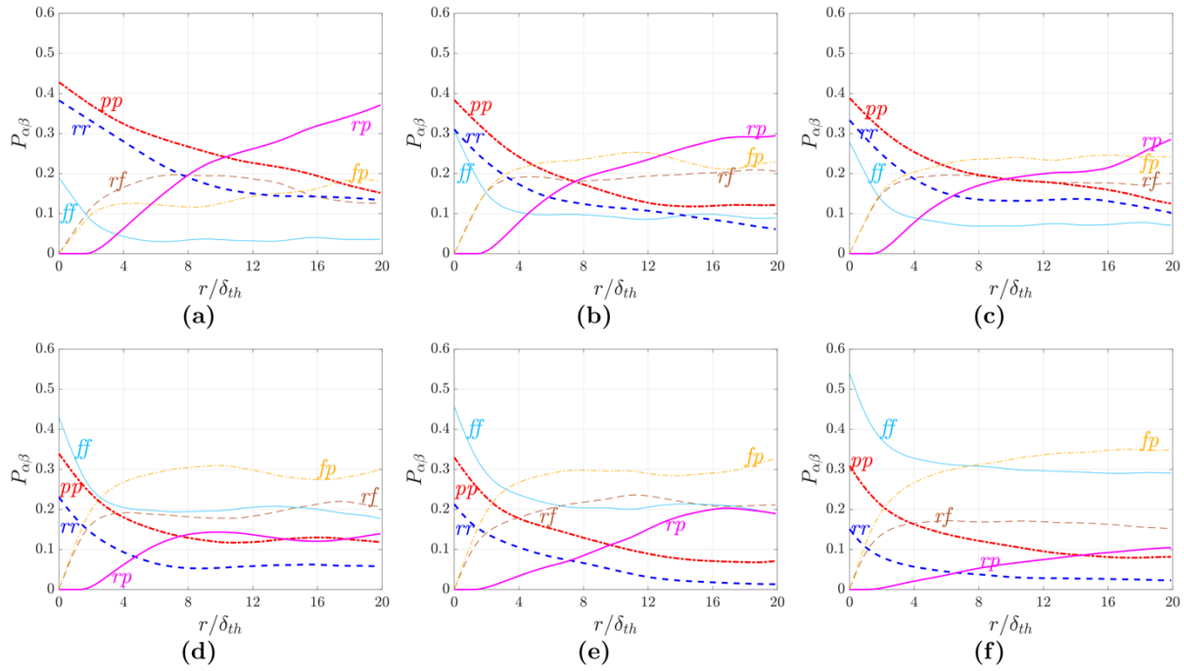

Fig. 4: Variations of the probabilities for various events $P_{\alpha\beta}$ as a function of normalised separation distance r/δ_{th} for (a-f) cases A-F at $\bar{c} = 0.5$.

The reactant-reactant (rr) and product-product (pp) structure functions assume smaller magnitudes in comparison to all the conditioned structure functions of $D_{11,T}^{\alpha\beta}(r)$ for cases A and B, see the left Figs 1a and 1b. This behaviour is consistent with the previous findings in the strict flamelet regime (i.e. $Ka < 1.0$).[3,5] The rr and pp components of $D_{11,T}(r)$ are least affected by the heat release and the rr component of $D_{11,T}(r)$ assumes the lowest magnitude among the conditioned structure function components in case A, whereas the pp component of $D_{11,T}(r)$ remains comparable to the rr component in case B. By contrast, the pp component of $D_{11,T}(r)$ assumes the lowest magnitude in cases C-F. It is apparent that the magnitude of velocity fluctuations increase across the flame brush in case A due to thermal expansion effects, whereas just the opposite behaviour has been observed in cases D-F, as the effects of thermal expansion are eclipsed by the influences of the background turbulence and viscous dissipation for cases with $u'/S_L \gg 1$ and $Ka > 1$.[22,23] This behaviour can be confirmed from Fig. 5, where the variation of the apparent turbulent kinetic energy $\tilde{k} = \overline{\rho u_i'' u_i''}/2\bar{\rho}$ with $\bar{c}$ across the flame brush is shown for all cases considered here. In case A, the level of velocity fluctuations gets augmented within the flame brush due to thermal expansion. In cases B-D, a local rise in $\tilde{k}$ in the region of the

flame brush where thermal expansion effects are strong can be seen following a decay of $\tilde{k}$ from the unburned gas side of the flame brush. By contrast, in cases E and F, $\tilde{k}$ decays monotonically from the unburned gas side of the flame brush due to the reduction of forcing and viscous dissipation. Thus, the disappearance of small-scale eddies due to the decay of turbulence and higher kinematic viscosity[70] in the burned gases is responsible for the weakened role of $D_{11,T}(r)$ components conditioned on products.

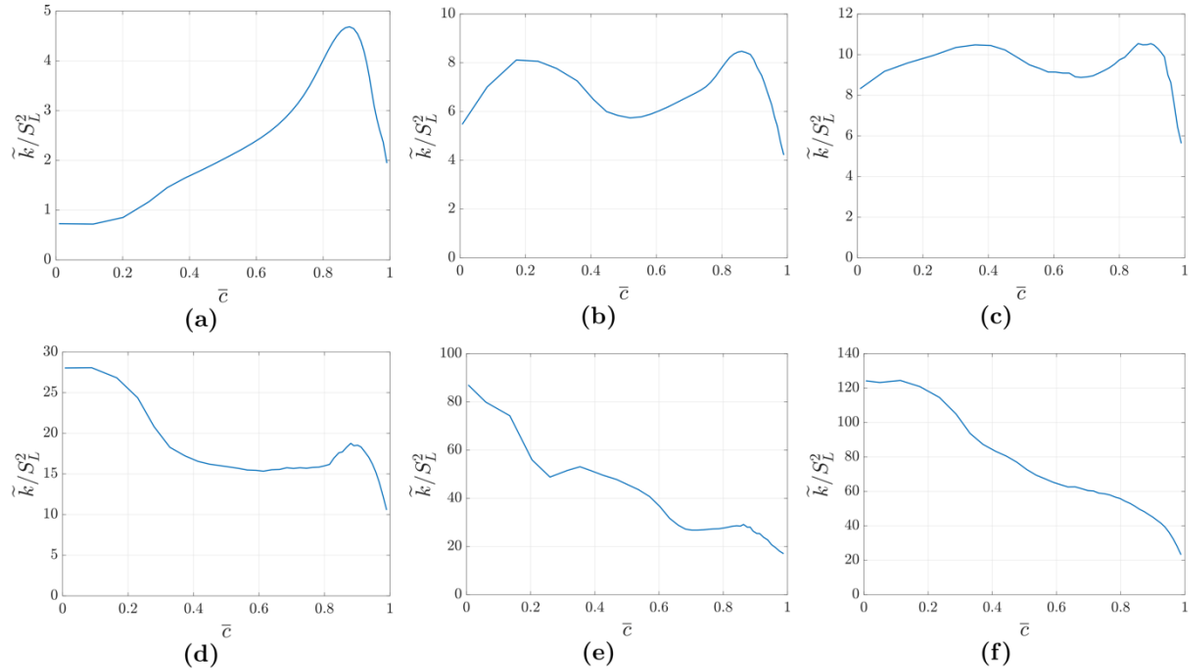

Fig. 5: Variations of normalised turbulent kinetic energy $\tilde{k}/S_L^2$ with $\bar{c}$ for (a-f) cases A-F.

The augmentation of velocity fluctuations due to thermal expansion in case A (and in case B for some values of r) acts to increase the magnitude of the pp component of $D_{11,T}(r)$ in comparison to the corresponding rr component. By contrast, the decay of turbulence across the flame is responsible for the higher magnitude of the rr component of $D_{11,T}(r)$ in comparison to the corresponding pp component in cases C-F. The rp component of $D_{11,T}(r)$ assumes the maximum magnitude in cases A and B, which is followed by the magnitudes of the fp, ff and rf components. This is a consequence of the strong effects of thermal expansion due to heat release in cases A and B and thus the maximum velocity difference can be expected between reactants and products, while the velocity difference is likely to be lowest for the structure functions associated with reactants due to the combination of weak

turbulence and weak thermal expansion effects. However, this behaviour changes for the cases with higher u'/S_L and Ka values (e.g. cases C-F). In cases C-F, the magnitude of the rr component of $D_{11,T}(r)$ remains comparable to that of the rp component and their magnitudes are followed by the magnitudes of fp, rf, ff and pp components. This is a consequence of combined effects of thermal expansion and weakening of turbulence from the reactants to the products side of the flame. In all cases, the rp component of $D_{11,T}(r)$ increases with r, and this can be attributed to a mechanism [28,71], which can be explained in the following manner.[9,11] If $\vec{x}_A$ associated with the unburned reactants is kept unchanged and $\vec{x}_B$ associated with the products is modified by increasing the transverse distance r, the axial product flow coming to point B is likely to significantly accelerate (the acceleration is inversely proportional to the fluid density) longer in the distance under axial pressure gradient and thus the axial velocity difference is likely to be higher in magnitude.

The magnitudes of rr, rf and rp components of $D^*_{11,T}(r)$ remain leading order contributors for all cases considered here and their relative magnitudes change from one case to another depending on relative influences of thermal expansion and fluid turbulence. In cases A, C, D and E, the rr component of $D^*_{11,T}(r)$ assumes the highest magnitude, whereas the magnitudes of rp and rf components play leading roles in case B. For all cases, the pp component of $D^*_{11,T}(r)$ remains negligible, because $\left(\rho_p/\rho_0\right)^2 \ll 1$. The aforementioned behaviours of $D^{\alpha\beta *}_{11,T}(r)$ are in contrast to the statistical behaviours of $D^{\alpha\beta}_{11,T}(r)$, due to significant density variations within premixed flames. Moreover, the leading order roles of the rr, rf and rp components of $D^*_{11,T}(r)$ is consistent with the importance of the leading edge of the flamelet in turbulent premixed combustion.

The differences in the magnitudes of $D^{\alpha\beta}_{23,T}(r)$ are smaller than those of $D^{\alpha\beta}_{11,T}(r)$. This behaviour arises from the fact that $\langle \partial p/\partial x_2 \rangle = 0$ and $\langle \partial p/\partial x_3 \rangle = 0$ in this flow configuration, which suggests that the flamelets normal to x_2-direction (x_3-direction) do not induce any pressure gradient in the x_3-direction (x_2-direction). As a result, the effects of thermal expansion on the structure function $D^{\alpha\beta}_{23,T}(r)$ are

relatively weaker than in the case of $D_{11,T}^{\alpha\beta}(r)$, which is consistent with previous findings.[9,11] However, thermal expansion effects are still present in $D_{23,T}^{\alpha\beta*}(r)$. The magnitudes of the rr, rf and rp components of $D_{23,T}^{*}(r)$ remain leading order contributors and the magnitude of the pp component remains negligible for all cases considered here.

The behaviours of the structure functions $D_{23,L}^{\alpha\beta}(r)$ for different cases are considerably different. In case A, the rp component starts to assume non-zero values in a discontinuous manner. A comparison between Figs. 3 and 4 indicates that this discontinuous jump in the rp component of $D_{23,L}(r)$ in case A takes place because the probability P_{rp} remains zero for small values of r. A similar behaviour was also reported by Sabelnikov et al. [9,11] The smallest value of r at which P_{rp} assumes non-zero value decreases with increasing turbulence intensity (i.e. $r/\delta_{th} = 1.7, 1.4, 1.3, 1.2, 1.1$ and 0.9 in cases A-F respectively) and the discontinuous jump in the rp component of $D_{23,L}(r)$ at small values of r is less pronounced for cases B-E. This discontinuity is observed but less pronounced in Figs. 1 and 2 because the magnitudes of the rp components of $D_{11,T}$ and $D_{23,T}$ remain small and show increasing trends with increasing r in contrast to the rp component of $D_{23,L}$ for case A, which shows a decreasing trend with increasing r. A close inspection of Figs. 1-3 also reveals discontinuities in the variations of the rp components of $D_{11,T}^{*}$, $D_{23,T}^{*}$ and $D_{23,L}^{*}$.

There are significant differences between different conditioned components in case A (especially, *rp* or *pp* and other components), whereas this difference becomes progressively less evident in cases B-F. This is a consequence of the weakening of the relative strength of the thermal expansion effects from case A to case F as one moves from the wrinkled flamelets regime to the thin reaction zones regime. The difference in the regime of the combustion is also responsible for the marked differences in the behaviours of $D_{23,L}^{\alpha\beta}(r)$ between cases A (representing the wrinkled flamelets regime) and B (representing the thin reaction zones regime).

In case A, the rp component of $D_{23,L}(r)$ decreases with increasing r, whereas this component increases and then assumes a value which does not change appreciably with r for other cases. In case A, the flame imparts significant influences on the underlying turbulent flow field and creates the mean pressure gradient $\langle \partial p/\partial x_1 \rangle$ only in the direction of mean flame propagation (i.e. x_1-direction) and this pressure gradient does not affect the flow in x_2 and x_3 directions. This suggests that the axial velocity in constant-density products are accelerated by $\langle \partial p/\partial x_1 \rangle$ in case A and thus the transverse velocities decrease to satisfy the continuity relation, which gives rise to a decrease in the rp component of $D_{23,L}(r)$ with increasing r. In the thin reaction zones regime cases C-F, the misalignment between the flamelet normal direction and the mean direction of flame propagation increases. As a result, the local flame normal pressure gradient in these cases is not only limited to x_1-direction and a component of the flame-induced pressure gradient also remains locally active in x_2 and x_3 directions. Furthermore, the underlying background turbulent flow field in cases C-F also induces appreciable local pressure gradients in the transverse directions, which also play some role in sustaining the magnitude of the rp component of $D_{23,L}(r)$ with increasing r in these cases. The pp component of the structure function $D_{23,L}(r)$ assumes a significantly greater value than the rr component in case A due to relatively strong thermal expansion effects in this case, as described earlier. By contrast, the rr component is of greater magnitude than the pp component in cases B-F due to the decay in turbulence intensity across the flame in these cases. The effects of thermal expansion manifest themselves also in the variations of $D_{23,L}^{\alpha\beta*}(r)$ and it can also be seen from Fig. 3 that the rr, rf and rp components of $D_{23,L}^{*}(r)$ remain leading order contributors and the magnitude of the pp component remains negligible for this structure function.

The statistical behaviours of the structure functions and their components also depend on the wrinkling of the reaction progress variable c isosurfaces in premixed turbulent combustion. The maximal and minimal values of the three components of the flame normal vector $\vec{N} = -\nabla c/|\nabla c|$ conditional on $\bar{c}$ across the flame brush are shown in Fig. 6. It is evident from Fig. 6 that there is a finite possibility of finding $|N_2| \approx 1$ or $|N_3| \approx 1$ within the flame brush. This tendency can be seen for cases A-B for $\bar{c} > 0.2$, whereas the possibility of finding $|N_2| \approx 1$ or $|N_3| \approx 1$ is observed throughout the flame brush in

cases C-F due to the greater extent of flame wrinkling for large values of u'/S_L. This suggests that the flamelets can be locally normal to x_2 or x_3 direction and, hence, locally parallel to x_1 and x_3 or x_2, direction respectively, which explains low (when compared to $(\tau S_L)^2$) jump in the rp component of $D_{23,T}$ at small distances in cases A-D, see Fig. 2. Otherwise, the difference in velocity component u_3 (u_2) in x_2-direction (x_3-direction) would have scaled with the velocity jump across the laminar flame (i.e. τS_L) at least for the flames in cases A-B where the flamelet assumption is expected to hold.

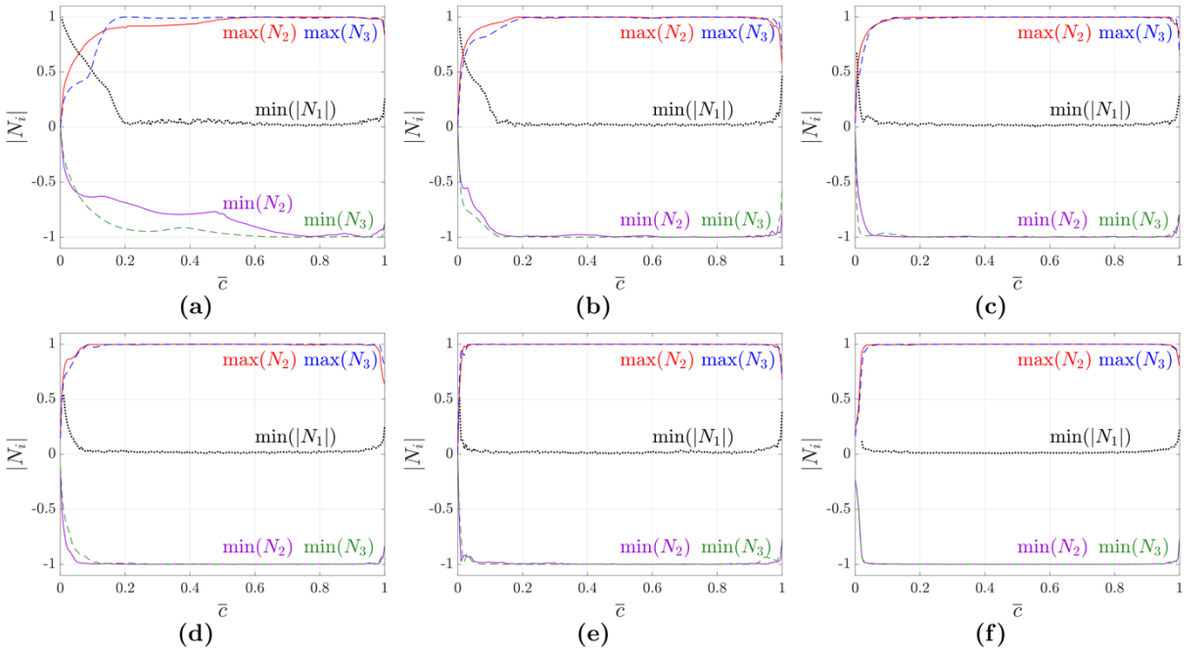

Fig. 6: Minimal and maximal values of the transverse components of the unit normal vector $\vec{N} = -\nabla c/|\nabla c|$ found for each transverse plane corresponding to $\bar{c}$ =constant for (a-f) cases A-F.

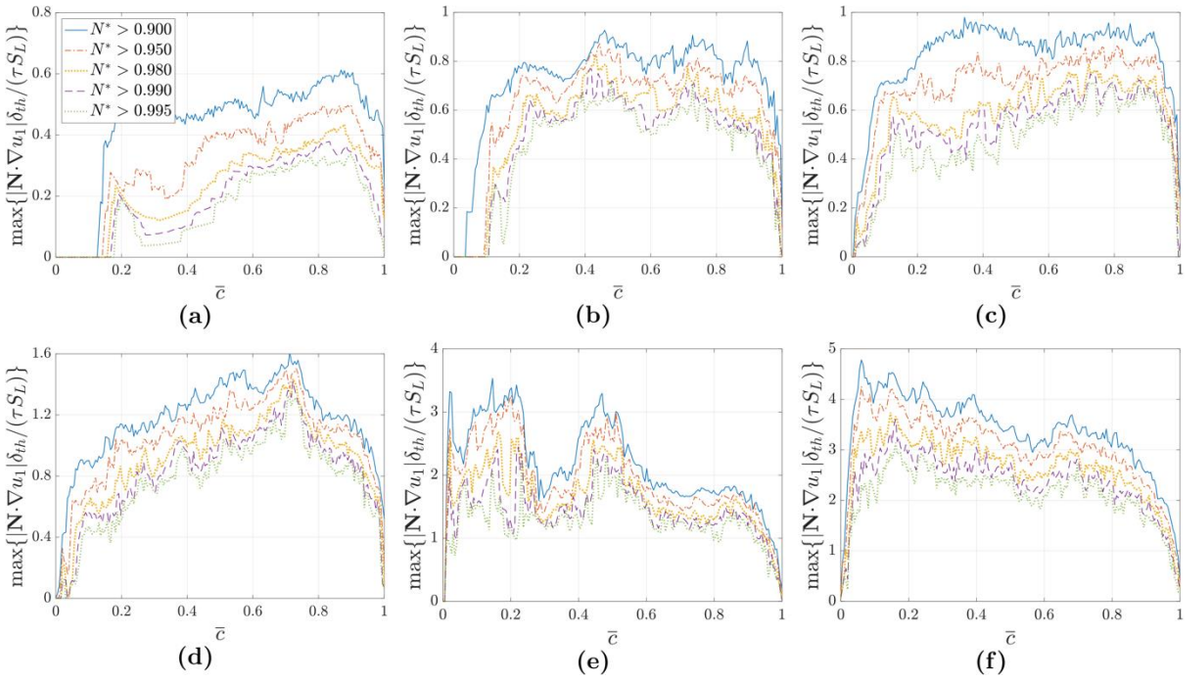

Fig. 7: Maximal (over each transverse plane at $\bar{c}$) values of $|\vec{N}\cdot\nabla u_1|\delta_{th}/\tau S_L$ for $|N_2| \geq N^*$ and/or $|N_3| \geq N^*$ for different threshold values of N^*, as specified in legends, for (a-f) cases A-F.

At low distances r comparable with the thickness δ_{th} the rp component of $D_{11,T}$ also assumes a comparable magnitude to that of $D_{23,L}$ (cf. Figs. 1 and 3), which suggests that there can be significant variation of the axial velocity u_1 when it is locally tangential to the flamelets. This can be substantiated from Fig. 7, which shows that the maximal magnitudes of the normal gradient of the locally tangential velocity (i.e. $|\vec{N}\cdot\nabla u_1|$ for either $|N_2| > N^*$ or $|N_3| > N^*$ where N^* is a threshold value close to unity) remain substantial in turbulent premixed flames. Furthermore, the magnitude of $\vec{N}\cdot\nabla u_1$ remains comparable to the corresponding value for laminar premixed flame (i.e. $\tau S_L/\delta_{th}$) for small values of u'/S_L and it has been found to increase with increasing u'/S_L. This can further be substantiated from Fig. 8 where the PDFs of $|\vec{N}\cdot\nabla u_1|\delta_{th}/\tau S_L$ for either $|N_2| \geq 0.95$ or $|N_3| \geq 0.95$ indicate that the probability of finding a notable value remains significant for all cases. This suggests that the velocity variations in turbulent flamelets might not be adequately modelled by the corresponding laminar flame expressions[36,37,71,72] and such assumptions are likely to be increasingly invalid for large values of u'/S_L. These results are not only in accordance with the previous findings[9,11,73] for the flames in the corrugated flamelets regime but also extend those findings for the flames in the thin reaction zones regime.

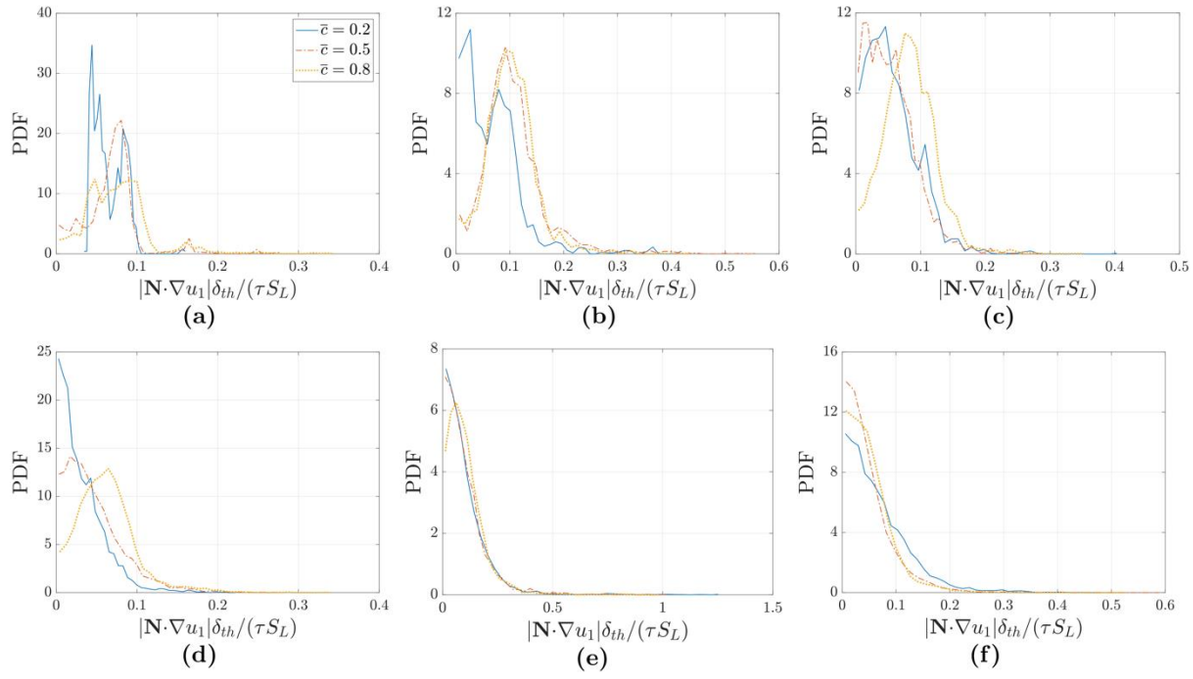

Fig. 8: PDFs of $|\vec{N}\cdot\nabla u_1|\delta_{th}/\tau S_L$ for either $|N_2| \geq 0.95$ or $|N_3| \geq 0.95$ for different values of $\bar{c}$ for (a-f) cases A-F.

Since the flame propagates into unburned reactants, the flame acceleration due to turbulence is mainly controlled by the turbulence in the reactants. Accordingly, the structure functions conditioned on the reactants provide key insights into flame-turbulence interaction. The local velocity fields and pressure perturbations induced by combustion are likely to affect the flame-turbulence interaction on the reactant side. To emphasize such effects, the variations of $D_{23,L}^{rr}/k_R$ with r/δ_{th} for different values of $\bar{c}$ (i.e. different distances from the leading edge) are shown in Fig. 9 for all cases where $k_R(x_1,t) = 0.5\langle u_i u_i(\vec{x},t) I_r(\vec{x},t)\rangle / P_r(x_1,t)$ is the turbulent kinetic energy conditioned upon reactants. It is evident from Fig. 9 that the appropriately normalised $D_{23,L}^{rr}$ increases with $\bar{c}$ for all cases, including case E characterized by u'/S_L as large as 10. It is admitted that $D_{23,L}^{rr}(\vec{r},t)$ could be affected by variable-density zones that the vector $\vec{r}$ crosses, which is certainly possible for sufficiently large r. However, in Fig. 9, the highlighted effect is also observed at r comparable with δ_{th}. These results show that, contrary to a common belief, the influence of combustion-induced thermal expansion on the incoming constant-density turbulent flow of unburned reactants is not restricted to weakly turbulent flames ($u'/S_L \approx 1$ and $Da \gg 1$) analysed recently [9,11], but also plays a substantial role even at $u'/S_L = 10$, $Ka \approx 20$, and

$Da < 1$. It can also be noted that Fig. 9 indicates an increase in the magnitude of such effects with u'/S_L.

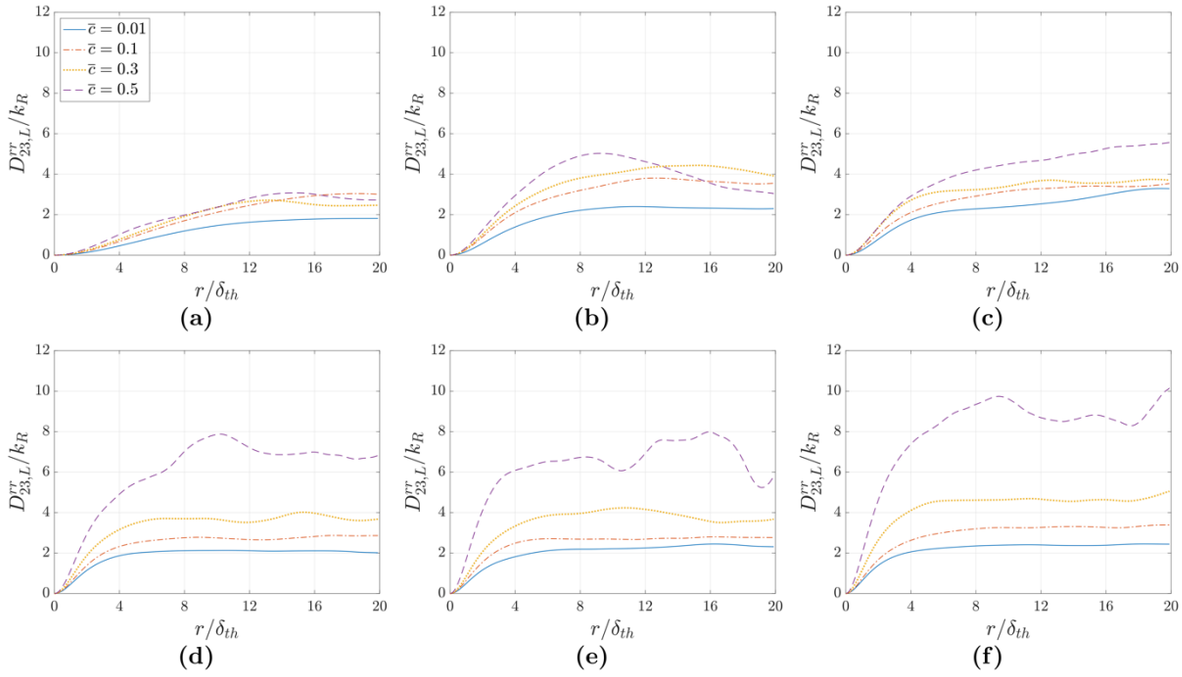

Fig. 9: Variations of $D^{rr}_{23,L}/k_R$ with r/δ_{th} for different values of $\bar{c}$ for (a-f) cases A-F.

To further study the above effects, the variation of the magnitude of the structure function $D^{rr}_{23,L}$ normalised by this function for $\bar{c} = 0.01$,i.e. $D^{rr}_{23,L}(r)/D^{rr}_{23,L}(r;\ \bar{c} = 0.01)$, is shown in Fig. 10. At first glance, Fig. 10 appears to contradict to the above claims by indicating a weak influence of $\bar{c}$ on the re-normalised $D^{rr}_{23,L}$ for cases C-E. However, it is worth noting that the simulated turbulence predominantly decays in the direction $x_1$within the flame brush, see Table 3, as the effects of forcing weaken with increasing $\bar{c}$. This gives rise to the mostly decreasing trend of the normalised turbulent kinetic energy conditioned upon reactants $k_R/k_R(\bar{c} = 0.01)$ with increasing $\bar{c}$, as $\bar{c}$ is a unique function of x_1 in this configuration. It is worth noting that cases A-C exhibit local augmentation of k_R due to thermal expansion effects close to the leading edge of the flame brush. This leads to higher values of $k_R/k_R(\bar{c} = 0.01)$ at $\bar{c} = 0.3$ than at $\bar{c} = 0.1$ for cases A and B but $k_R/k_R(\bar{c} = 0.01)$ values at $\bar{c} = 0.5$ remain smaller than the values at $\bar{c} = 0.3$ in these cases. The values of $k_R/k_R(\bar{c} = 0.01)$ decay monotonically with increasing $\bar{c}$ in cases C-F.

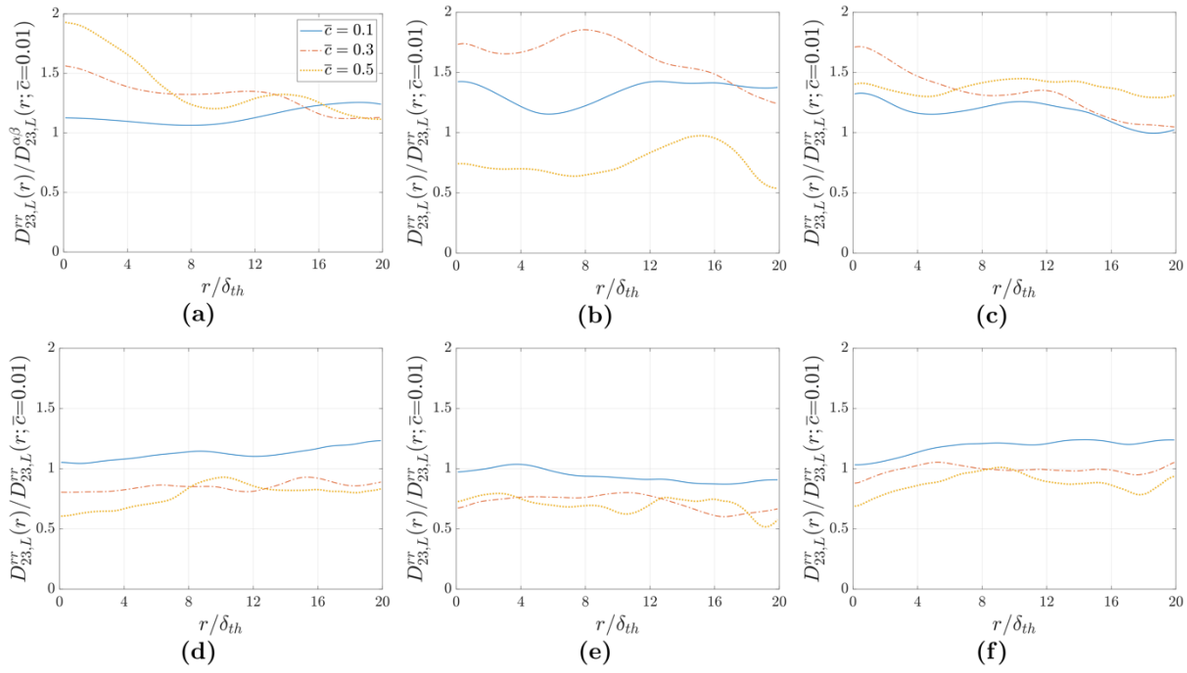

Fig. 10: Variations of the magnitude of the structure function $D^{rr}_{23,L}$ normalised by its value for $\bar{c} = 0.01$ (i.e. $D^{rr}_{23,L}(r)/D^{rr}_{23,L}(r;\ \bar{c} = 0.01)$ for (a-f) cases A-F.

Table 3 implies that if the thermal expansion effects were weak, the ratio of $D^{rr}_{23,L}(r;\bar{c})/D^{rr}_{23,L}(r;\ \bar{c} = 0.01)$ would have decreased with $\bar{c}$ similarly to the conditioned turbulent kinetic energy k_R in cases C-F. However, such a decrease is not observed in Figs. 10c-f, and thus, indicating significant importance of the thermal expansion effects in these cases. In case A, the decrease in k_R with $\bar{c}$ is weakly pronounced (see Table 3) and $D^{rr}_{23,L}(r)/D^{rr}_{23,L}(r;\ \bar{c} = 0.01)$ increases with increasing $\bar{c}$ in the mean reaction progress variable range given by $0.1 \leq \bar{c} \leq 0.5$. A similar trend has been observed for case B for $r/\delta_{th} \lessapprox 10$ and even for $r/\delta_{th} > 10$, the normalised structure function $D^{rr}_{23,L}(r)/D^{rr}_{23,L}(r;\ \bar{c} = 0.01)$ increases with increasing $\bar{c}$ in the mean reaction progress variable range given by $0.1 \leq \bar{c} \leq 0.3$. The observations from Figs. 9 and 10 indicate that the thermal expansion effects due to chemical heat release have significant influences on the two-point velocity statistics of incoming non-reacting turbulent flows in premixed flames. A similar behaviour can be obtained if the rr component of $D^{rr*}_{23,L}$ instead of $D^{rr}_{23,L}$ is considered because density does not change in the non-reacting mixture.

Case	$k_R/k_R(\bar{c}=0.01)$		
	$\bar{c}=0.1$	$\bar{c}=0.3$	$\bar{c}=0.5$
A	0.7090	0.7853	0.7103
B	0.7239	0.9196	0.7753
C	0.8815	0.8618	0.7164
D	0.8353	0.4674	0.2463
E	0.7238	0.3976	0.2149
F	0.8643	0.4899	0.2447

Table 3. Variation in turbulent kinetic energy conditioned to the reactants as a ratio of its value at $\bar{c}=0.01$ (i.e. $k_R/k_R(\bar{c}=0.01)$) at various $\bar{c}$ for cases A-F.

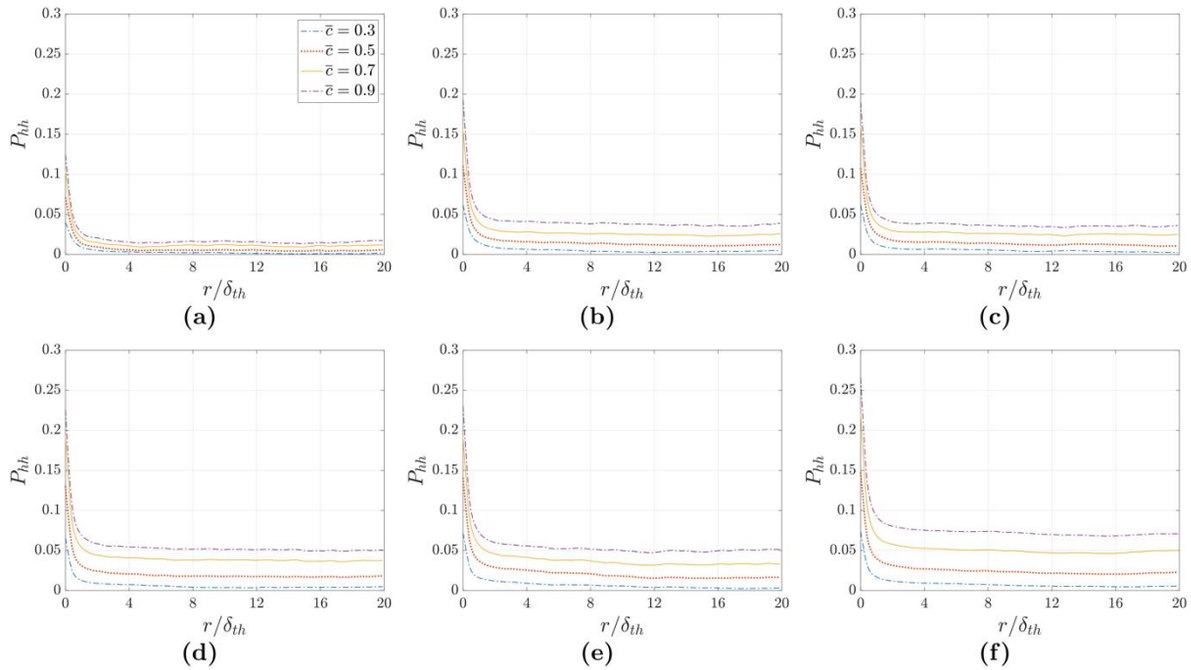

Fig. 11: Probability of finding the entire segment [A; B] within heat release zones ($0.75 \leq c \leq 0.95$) for different values of $\bar{c}$ for (a-f) cases A-F.

Finally, it is worthwhile to consider the statistical behaviours of the structure functions D_{ij}^{hh} and D_{ij}^{hh*} conditioned on the heat release zone, which is taken to be the region corresponding to $0.75 \leq c \leq 0.95$. The separation between two points needs to be small in order to get two points in the heat release zone and thus the probability of finding two points in the heat release zone P_{hh} drops sharply with distance r/δ_{th}. This can be substantiated from Fig. 11, where the variations of P_{hh} with r/δ_{th} are shown. Figure 11 further shows that the value of P_{hh} where it settles after decaying from the leading edge increases

with increasing u'/S_L. This is a consequence of the enhancement of flame wrinkling with increasing u'/S_L, which leads to an increase in the probability of finding two points in the heat release zone.

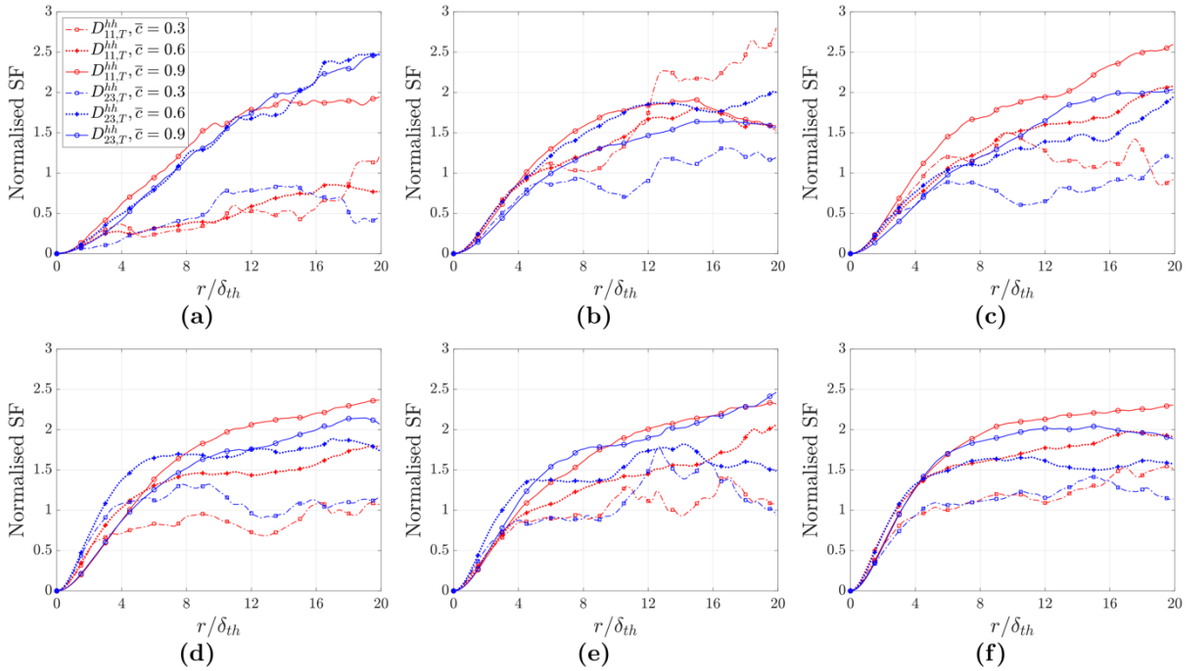

Fig. 12: Variations of the normalised transverse structure functions $D^{hh}_{11,T}/\overline{u_1'^2}$ and $2D^{hh}_{23,T}/\{\overline{u_2'^2} + \overline{u_3'^2}\}$ as a function of the normalised r/δ_{th} for (a-f) cases A-F for different values of $\bar{c}$.

Figure 12 indicates that the maximal normalised values of transverse structure functions $D^{hh}_{11,T}/\overline{u_1'^2}$ and $2D^{hh}_{23,T}/\{\overline{u_2'^2} + \overline{u_3'^2}\}$ remain comparable for all cases considered here. However, for small values of separation distance r, the normalised structure function $D^{hh}_{11,T}/\overline{u_1'^2}$ increases more rapidly than $2D^{hh}_{23,T}/\{\overline{u_2'^2} + \overline{u_3'^2}\}$ in cases with small u'/S_L (e.g. cases A-C) where the baroclinic torque (i.e. $(\nabla\rho \times \nabla p)/\rho^2$) plays a key role in the vorticity $\vec{\omega} = \nabla \times \vec{u}$ transport and enhances ω_2 and ω_3 .[13-17,74,75] By contrast, the vorticity transport in cases with $u'/S_L \gg 1$ (e.g. cases D-F) is governed by vortex-stretching, dilatation and molecular dissipation terms.[14-17,74,75] In these cases, enstrophy drops monotonically from the leading edge and the components ω_1, ω_2 and ω_3 behave in a similar manner within the flame.[14-16] This further suggests that the effects of anisotropy can be significant for flames in the wrinkled flamelets and corrugated flamelets regime but these effects progressively weaken in the thin reaction zones regime with increasing Karlovitz number.

V. CONCLUSIONS

The statistical behaviours of the second-order velocity structure functions and its components conditioned upon various events (e.g. (i) two points in reactants, (ii) two points in products, (iii) one point in reactants and the other in products, (iv) one point in the reacting mixture and the other in reactants, (v) one point in the reacting mixture and the other in products and (vi) two points in the heat release zone) have been analysed using a DNS database for statistically planar premixed flames under forced unburned gas turbulence spanning from the wrinkled flamelets to the thin reaction zones regime. The structure functions and its various conditioned components have also been analysed for density-weighted velocities.

It has been found that, in all studied cases, the thermal expansion induced by heat release due to combustion significantly affects the behaviour of the conditioned structure functions. The conditioned components differ from one-other and from the conventional unconditioned mean structure functions. The use of the density-weighted structure functions does not substantially reduce these effect magnitudes.

The structure functions conditioned to constant-density unburned reactants at both points and normalised using the rms velocity conditioned to the reactants have the largest magnitude at large $\bar{c}$, with this trend being not weakened with increasing u'/S_L. These results indicate that, contrary to a common belief, combustion-induced thermal expansion can significantly affect the incoming constant-density turbulent flow of unburned reactants even at u'/S_L and Ka as large as 10 and 18, respectively. This is one of the most important findings from this work. It is difficult to conclusively predict when the thermal expansion effects are not going to be strong based on limited available data but it is, however, safe to claim that these effects survive in the thin reaction zones regime for moderate values of Damköhler number. The flame normal acceleration can be scaled using $\tau S_L/\delta_{th}$ according to the laminar flamelet theory and thus the ratio of flame normal acceleration to large scale turbulent straining ($\sim u'/l$), can be taken to be proportional to $\tau S_L l/u'\delta_{th} = \tau Da$. For all cases considered here, τDa

remains of the order of unity (i.e. $\tau Da \sim O(1)$) and therefore the thermal expansion effects play key roles in these flames. Thus, one has to consider very low values of Da in order to obtain a situation where the thermal expansion effects become too weak to impart any influence on the incoming turbulent flow of unburned reactants.

Furthermore, the statistical behaviours of the structure functions motivated some statistical analysis related to flame normal components and flame normal velocity gradient, which eventually revealed that the normal gradient of the tangential (to the local flame) velocity component can be substantial and it increases with increasing u'/S_L. This is contrary to the common modelling assumption in the flamelet regime, which considers that the velocity jump only takes place in the local flame normal direction and the tangential velocity remains unaffected.

The strong effects of baroclinic torque in the small u'/S_L cases representing the wrinkled flamelets and corrugated flamelets regimes can have significant anisotropic impacts on the longitudinal and transverse structure functions. However, the anisotropic effects induced by baroclinic torque weaken progressively with increasing u'/S_L in the thin reaction zones regime.

The behaviour of conditional second-order structure functions (e.g. (e.g. $D_{23,L}^{rr}(r)/D_{23,L}^{rr}(r;\ \bar{c}=0.01)$, $D_{23,L}^{rr}(r)/k_R$) provides a measure of the strength of underlying thermal expansion effects and these statistics can be used to assess if the thermal expansion effects play an important role in a given flow situation. The current findings suggest that the thermal expansion effects and timescales associated with it cannot be neglected in the thin reaction zones regime and these effects become unimportant only for extremely large (small) values of Karlovitz number (Damköhler number). The analysis of structure function statistics in premixed flames and its application in combustion modelling are in a rudimentary stage and beyond the scope of this work but will form the basis of future investigations.

ACKNOWLEDGEMENTS

The authors are grateful to EPSRC for funding and to ARCHER and Rocket HPC (Newcastle) for computational assistance. The fourth author (AL) is grateful for funding to Combustion Engine Research Centre (CERC).

REFERENCES

[1]A.S. Monin, A. M. Yaglom, Statistical Fluid Mechanics: Mechanics of Turbulence, Vol. 2. The MIT Press, 1975.

[2]U. Frisch, Turbulence: The Legacy of A.N. Kolmogorov. Cambridge University Press, 1995.

[3]S.B. Pope, Turbulent flows, 1st Edition, Cambridge University Press, 2000.

[4]P. A. Davidson, Turbulence: An Introduction for Scientists and Engineers, 2nd edn., Oxford University Press, 2005.

[5]H. Kolla, E.R. Hawkes, A.R. Kerstein, N. Swaminathan, J. H. Chen, On velocity and reactive scalar spectra in turbulent premixed flames. J. Fluid Mech. 75, 456–487, 2014.

[6]C. A.Z. Towery, A.Y. Poludnenko, J. Urzay, J. O'Brien, M. Ihme, P.E. Hamlington, Spectral kinetic energy transfer in turbulent premixed reacting flows. Phys. Rev. E 93, 053115, 2016.

[7] J. O'Brien, C. A.Z. Towery, P.E. Hamlington, M. Ihme, A.Y. Poludnenko, J. Urzay, The cross-scale physical-space transfer of kinetic energy in turbulent premixed flames. Proc. Combust. Inst. 36, 1967–1975, 2017.

[8] J. Kim, M. Bassenne, C. A.Z. Towery, P.E. Hamlington, A.Y. Poludnenko, J. Urzay, The cross-scale physical-space transfer of kinetic energy in turbulent premixed flames. J. Fluid. Mech. 848, 78-116, 2018.

[9]V.A. Sabelnikov, A. L. Lipatnikov, S. Nishiki, T. Hasegawa, Application of conditioned structure functions to exploring influence of premixed combustion on two-point turbulence statistics, Proc. Combust. Inst., 37, 2433-2441, 2019.

[10]S.H.R. Whitman, C. Towery, A.Z. Poludnenko, P.E. Hamlington, Scaling and collapse of conditional velocity structure functions in turbulent premixed flames, Proc. Combust. Inst., 37, 2433-2441, 2019.

[11]V.A. Sabelnikov, A. L. Lipatnikov, S. Nishiki, T. Hasegawa, Conditioned structure function method for studying influence of combustion-induced thermal expansion on two-point turbulence statistics in premixed flames, J. Fluid Mech., 867, 45-76, 2019.

[12]N. Chakraborty, Alignment of vorticity with strain rates in turbulent premixed flames, Eur. J. Mech. B-Fluids, 46, 201-220, 2014.

[13]A. L. Lipatnikov, S. Nishiki, T. Hasegawa, A direct numerical simulation study of vorticity transformation in weakly turbulent premixed flames. Phys. Fluids 26, 105104, 2014.

[14]N. Chakraborty, I. Konstantinou, A. Lipatnikov, Effects of Lewis number on vorticity and enstrophy transport in turbulent premixed flames, Phys. Fluids, 28,015109, 2016.

[15]C. Dopazo, L. Cifuentes, N. Chakraborty, Vorticity budgets in premixed combusting turbulent flows at different Lewis numbers, Phys. Fluids, 29, 045106, 2017.

[16]N. Chakraborty, L. Wang, I. Konstantinou, M. Klein, Vorticity statistics based on velocity and density-weighted velocity in premixed reactive turbulence, J. Turb., 18, 9, 2017.

[17]V. Papapostolou, D.H. Wacks, M. Klein, N. Chakraborty, H.G. Im, Enstrophy transport conditional on local flow topologies in different regimes of premixed turbulent combustion, Scientific Reports, 7, 11545, 2017.

[18] A.N. Lipatnikov, V. Sabelnikov, S. Nishiki, T. Hasegawa, Does flame-generated vorticity increase turbulent burning velocity? Phys. Fluids, 30, 081702, 2018.

[19] A.N. Lipatnikov, V. Sabelnikov, S. Nishiki, T. Hasegawa, A direct numerical simulation study of the influence of flame-generated vorticity on reaction-zone-surface area in weakly turbulent premixed combustion, Phys. Fluids, 31, 055101, 2019.

[20]S. Zhang, C.J. Rutland, Premixed flame effects on turbulence and pressure-related terms, Combust. Flame 102, 447-461, 1995.

[21]S. Nishiki, T. Hasegawa, R. Borghi, R. Himeno, Modelling of flame generated turbulence based on direct numerical simulation databases, Proc. Combust. Inst. 29, 2017-2022, 2002.

[22]N. Chakraborty, M. Katragadda, R.S. Cant, Statistics and modelling of turbulent kinetic energy transport in different regimes of premixed combustion, Flow Turb. Combust., 87,205-235, 2011.

[23]N. Chakraborty, M. Katragadda, R.S. Cant, Effects of Lewis number on turbulent kinetic energy transport in turbulent premixed combustion, Phys. Fluids, 23, 075109, 2011.

[24]Z. Wang and J. Abraham, Effects of Karlovitz number on turbulent kinetic energy transport in turbulent lean premixed methane/air flames, Phys. Fluids 29, 085102, 2017.

[25]B. Karlovitz, D. W. Denniston, Jr., D.H. Knapschaefer, F.E. Wells, Studies on turbulent flames, Proc. Combust. Inst. 4, 613-620, 1953.

[26]K. N. C. Bray, P.A. Libby, Interaction effects in turbulent premixed flames, Phys. Fluids A 19, 1687, 1976.

[27]J. Chomiak, J. Nisbet, Modelling variable density effects in turbulent flames, Combust. Flame 102, 371-386, 1995.

[28]A. C. Scurlock, J. H. Grover, Propagation of turbulent flames. Proc. Combust. Inst.,4, 645-658, 1953.

[29]P. Moreau, A. Boutier, Laser velocimeter measurements in a turbulent flame, Proc. Combust. Inst. 16, 1747-1756, 1977.

[30]J.B. Moss, Simultaneous measurements of concentration and velocity in an open premixed flame, Combust. Sci. Technol. 22, 119-129, 1980.

[31]R. Borghi, D. Escudie, Assessment of a theoretical model of turbulent combustion by comparison with a simple experiment, Combust. Flame, 56, 149-164, 1984.

[32]B. Coriton and J. H. Frank, Experimental study of vorticity-strain rate interaction in turbulent partially premixed jet flames using tomographic particle image velocimetry, Phys. Fluids 28, 025109,2016.

[33]H. Wang, E. R. Hawkes, and J. H. Chen, Turbulence-flame interactions in DNS of a laboratory high Karlovitz premixed turbulent jet flame, Phys. Fluids 28, 095107,2016.

[34] G. Nivarti and R. S. Cant, Scalar transport and the validity of Damköhler's hypotheses for flame propagation in intense turbulence, Phys. Fluids 29, 085107,2017.

[35]A. N. Lipatnikov, Can we characterize turbulence in premixed fames, Combust. Flame, 156, 1242-1247, 2009.

[36]A.N. Lipatnikov, J. Chomiak, Effects of premixed flames on turbulence and turbulent scalar transport. Prog. Energy Combust. Sci. 36, 1-102, 2010.

[37]V.L. Sabelnikov, A.N. Lipatnikov, Recent advances in understanding of thermal expansion effects in premixed turbulent flames, Ann. Rev. Fluid Mech., 49, 91-117, 2017.

[38]A.N. Kolmogorov, The local structure of turbulence in incompressible viscous fluid for very large Reynolds number. Dokl. Akad. Nauk SSSR 30, 299-303, 1941.

[39]M. Lesieur, O. Metais, P. Comte, Large-Eddy Simulations of Turbulence. Cambridge University Press, 2005.

[40]N. Peters, Turbulent combustion, 1st Edition, Cambridge University Press, 2000.

[41]U. Ahmed, N. Chakraborty, M. Klein, Insights into the bending effect in premixed turbulent combustion using the Flame Surface Density transport, Combust. Sci. Technol., DOI: 10.1080/00102202.2019.1577241, 2019.

[42]U. Ahmed, M. Klein, N. Chakraborty, On the stress-strain alignment in premixed turbulent flames, Scientific Reports, 9, 5092, 2019.

[43]P.A. Libby, On the prediction of intermittent turbulent flows, J. Fluid Mech., 68, 273-295, 1975.

[44] P.A. Libby, Prediction of the intermittent turbulent wake of a heated cylinder, Phys. Fluids, 19, 494, 1976.

[45]C. Dopazo, On conditioned averages for intermittent turbulent flows, J. Fluid Mech., 81, 433-438, 1977.

[46]C. Dopazo, E.E. O'Brien, Intermittency in free turbulent shear flow, Lecture Notes in Physics Turbulent Shear Flow I, 6-23, Ed. F. Durst et al., Springer Verlag, Berlin, 1978.

[47]E.E O'Brien, C. Dopazo, Behavior of conditioned variables in free turbulent shear flows, H. Fiedler Ed., Structure and Mechanisms of Turbulence II., Lecture Notes in Physics, 76, 124-137, Springer-Verlag, New York, 1979.

[48]V.R. Kuznetsov, V. A. Sabelnikov, Turbulence and Combustion, Hemisphere Publ. Corp., 1990.

[49]K.W. Jenkins, R.S. Cant, Direct numerical simulation of turbulent flame kernels. In D. Knight & L. Sakell, (eds) Recent Advances in DNS and LES: Proceedings of the Second AFOSR Conference, Rutgers - The State University of New Jersey, New Brunswick, USA, 191–202 (Kluwer, Dordrecht, 1999), 1999.

[50]N. Chakraborty and S. Cant, Unsteady effects of strain rate and curvature on turbulent premixed flames in an inlet-outlet configuration, Combust. Flame, 137, 129-147, 2004.

[51]N. Chakraborty and R.S. Cant, Influence of Lewis Number on curvature effects in turbulent premixed flame propagation in the thin reaction zones regime, Phys. Fluids, 17,105105, 1-20, 2005.

[52]N. Chakraborty, Comparison of displacement speed statistics of turbulent premixed flames in the regimes representing combustion in corrugated flamelets and thin reaction zones, Phys. Fluids, 19,105109,2007.

[53]T. Echekki, J.H. Chen, Unsteady strain rate and curvature effects in turbulent premixed methane-air flames, Combust. Flame, 106, 184-202, 1996.

[54] N. Peters, P. Terhoeven, J.H. Chen, T. Echekki, Statistics of Flame Displacement Speeds from Computations of 2-D Unsteady Methane-Air Flames, Proc. Combust. Inst., 27,833-839, 1998.

[55]T. Echekki, J.H. Chen, Analysis of the Contribution of Curvature to Premixed Flame Propagation, Combust. Flame, 118, 303-311, 1999.

[56]N. Chakraborty and R.S. Cant, Effects of strain rate and curvature on Surface Density Function transport in turbulent premixed flames in the thin reaction zones regime, Phys. Fluids, 17, 65108, 2005.

[57]N. Chakraborty, M. Klein, Influence of Lewis number on the Surface Density Function transport in the thin reaction zones regime for turbulent premixed flames, Phys. Fluids, 20, 065102, 2008.

[58]N. Chakraborty, H. Kolla, R. Sankaran, E. R. Hawkes, J. H. Chen, N. Swaminathan, Determination of three-dimensional quantities related to scalar dissipation rate and its transport from two-dimensional measurements: Direct Numerical Simulation based validation, Proc. Combust. Inst., 34,1151-1162, 2013.

[59]N. Chakraborty, E.R. Hawkes, J.H. Chen, R.S. Cant, Effects of strain rate and curvature on Surface Density Function transport in turbulent premixed CH4-air and H2-air flames: A comparative study, Combust. Flame, 154,259-280,2008.

[60]Y.Gao, N. Chakraborty, M. Klein, "Assessment of sub-grid scalar flux modelling in premixed flames for Large Eddy Simulations: A-priori Direct Numerical Simulation", Eur. J. Mech. Fluids-B, 52, 97-108, 2015.

[61]M. Klein, C. Kasten, N. Chakraborty, N. Mukhadiyev, H.G. Im, "Turbulent scalar fluxes in Hydrogen-Air premixed flames at low and high Karlovitz numbers", Combust. Theor. Modell., 22, 1033-1048,2018.

[62]Y. Gao, N. Chakraborty, N. Swaminathan, "Algebraic closure of scalar dissipation rate for Large Eddy Simulations of turbulent premixed combustion", *Combust. Sci. Technol.*, 186, 1309-1337, 2014

[63]Y.Gao, Y. Minamoto, M. Tanahashi, N. Chakraborty, A priori assessment of scalar dissipation rate closure for Large Eddy Simulations of turbulent premixed combustion using a detailed chemistry Direct Numerical Simulation database, Combust. Sci. Technol., 188,1398-1423, 2016.

[64]A.A. Wray, Minimal storage time advancement schemes for spectral methods, unpublished report, NASA Ames Research Center, California, 1990.

[65]T. Poinsot, S.K. Lele, Boundary conditions for direct simulation of compressible viscous flows, J. Comp. Phys., 101, 104-129, 1992.

[66]M. Klein, N. Chakraborty, S. Ketterl, A comparison of strategies for Direct Numerical Simulation of turbulence chemistry interaction in generic planar turbulent premixed flames. Flow, Turbul. Combust. 99, 955–971, 2017.

[67]A.J. Aspden, M.S. Day, J.B., Turbulence-flame interactions in lean premixed hydrogen: transition to the distributed burning regime. J. Fluid Mech. 680, 287-320, 2011.

[68]A.Y. Poludnenko, E.S. Oran, The interaction of high-speed turbulence with flames: Global properties and internal flame structure. Combust. Flame, 157, 995-1011, 2010.

[69]B. Savard, G. Blanquart, Broken reaction zone and differential diffusion effects in high Karlovitz n-C7H16 premixed turbulent flames, Combust. Flame, 162, 2020-2033, 2015.

[70]T. Wabel, A.W. Skiba, J.F. Driscoll, Evolution of turbulence through a broadened preheat zone in a premixed piloted Bunsen flame from conditionally-averaged velocity measurements, Combust. Flame, 188, 13-27, 2018.

[71]P.A. Libby, K.N.C. Bray, Countergradient diffusion in premixed turbulent flames. AIAA J. 19, 205-213, 1981.

[72]K.N.C. Bray, Turbulent transport in flames, Proc. R. Soc. London A, 451, 231-256, 1995.

[73]A.N. Lipatnikov, V. Sabelnikov, S. Nishiki, T. Hasegawa, Combustion-induced local shear layers within premixed flamelets in weakly turbulent flows. Phys. Fluids, 30, 085101, 2018.

[74]P.E. Hamlington, J. Schumacher, W. J.A. Dahm, Local and nonlocal strain rate and vorticity alignment in turbulent flows, Phys. Rev. E., 77, 026303, 2008.

[75]P.E. Hamlington, A.Y. Poludnenko, E.S. Oran, Interactions between turbulence and flames in premixed reacting flows, Phys. Fluids, 23, 125111, 2011.

TABLES

Cases	u'/S_L	l/δ_{th}	Da	Ka	τ	Domain	Grid	Regime
A	1.0	3.0	3.0	0.58	4.5	$79.5\delta_{th} \times (39.8\delta_{th})^2$	$800 \times 400 \times 400$	Wrinkled/Corrugated flamelets
B	2.5	3.0	1.2	2.28	4.5	$79.5\delta_{th} \times (39.8\delta_{th})^2$	$800 \times 400 \times 400$	Corrugated flamelets
C	3.0	3.0	1.0	3.0	4.5	$79.5\delta_{th} \times (39.8\delta_{th})^2$	$800 \times 400 \times 400$	Thin reaction zones
D	5.0	3.0	0.6	6.5	4.5	$79.5\delta_{th} \times (39.8\delta_{th})^2$	$800 \times 400 \times 400$	Thin reaction zones
E	7.5	3.0	0.4	11.9	4.5	$79.5\delta_{th} \times (39.8\delta_{th})^2$	$800 \times 400 \times 400$	Thin reaction zones
F	10.0	3.0	0.3	18.3	4.5	$79.5\delta_{th} \times (39.8\delta_{th})^2$	$800 \times 400 \times 400$	Thin reaction zones

Table 1: The attributes of the DNS database considered for this analysis.

Case	$\frac{\max(D_{11,T})}{2\langle u'_1 u'_1\rangle}$	$\frac{\max(D_{23,T})}{\langle u'_2 u'_2\rangle + \langle u'_3 u'_3\rangle}$	$\frac{\max(D_{23,L})}{\langle u'_2 u'_2\rangle + \langle u'_3 u'_3\rangle}$
A	1.053	1.169	1.136
B	1.415	0.972	1.004
C	1.151	0.997	1.122
D	0.800	1.136	1.120
E	1.156	1.036	1.000
F	0.851	0.968	0.929

Table 2. Values of $\max(D_{11,T})/2\langle u'_1 u'_1\rangle$, $\max(D_{23,T})/\{\langle u'_2 u'_2\rangle + \langle u'_3 u'_3\rangle\}$, $\max(D_{23,L})/\{\langle u'_2 u'_2\rangle + \langle u'_3 u'_3\rangle\}$ for $\bar{c} = 0.5$.

Case	$k_R/k_R(\bar{c} = 0.01)$		
	$\bar{c} = 0.1$	$\bar{c} = 0.3$	$\bar{c} = 0.5$
A	0.7090	0.7853	0.7103
B	0.7239	0.9196	0.7753
C	0.8815	0.8618	0.7164
D	0.8353	0.4674	0.2463
E	0.7238	0.3976	0.2149
F	0.8643	0.4899	0.2447

Table 3. Variation in turbulent kinetic energy conditioned to the reactants as a ratio of its value at $\bar{c} = 0.01$ (i.e. $k_R/k_R(\bar{c} = 0.01)$) at various $\bar{c}$ for cases A-F.

FIGURE CAPTIONS

Fig. 1: Variations of normalised transverse conditioned structure functions (coloured lines) $D_{11,T}^{\alpha\beta}(r)/(\tau S_L)^2$ (left column) and $D_{11,T}^{\alpha\beta*}(r)/(\tau S_L)^2$ (right column) and mean unconditioned structure functions (black dots) $D_{11,T}(r)/(\tau S_L)^2$ (left column) and $D_{11,T}^{*}(r)/(\tau S_L)^2$ (right column) for axial velocities as a function of normalised separation distance r/δ_{th} for (a-f) cases A-F at $\bar{c} = 0.5$. Here, $D_{11,T}^{\alpha\beta*}(r)/(\tau S_L)^2$ and $D_{11,T}^{*}(r)/(\tau S_L)^2$ are normalised structure functions based on the density-weighted velocity $\vec{u}^* = \rho\vec{u}/\rho_0$.

Fig. 2: Variations of normalised transverse conditioned structure functions (coloured lines) $D_{23,T}^{\alpha\beta}(r)/(\tau S_L)^2$ (left column) and $D_{23,T}^{\alpha\beta*}(r)/(\tau S_L)^2$ (right column) and mean unconditioned structure functions (black dots) $D_{23,T}(r)/(\tau S_L)^2$ (left column) and $D_{23,T}^{*}(r)/(\tau S_L)^2$ (right column) for transverse velocities as a function of normalised separation distance r/δ_{th} for (a-f) cases A-F at $\bar{c} = 0.5$. Here, $D_{23,T}^{\alpha\beta*}(r)/(\tau S_L)^2$ and $D_{23,T}^{*}(r)/(\tau S_L)^2$ are normalised structure functions based on the density-weighted velocity $\vec{u}^* = \rho\vec{u}/\rho_0$.

Fig. 3: Variations of normalised longitudinal conditioned structure functions (coloured lines) $D_{23,L}^{\alpha\beta}(r)/(\tau S_L)^2$ (left column) and $D_{23,L}^{\alpha\beta*}(r)/(\tau S_L)^2$ (right column) and mean unconditioned structure functions (black dots) $D_{23,L}(r)/(\tau S_L)^2$ (left column) and $D_{23,L}^{*}(r)/(\tau S_L)^2$ (right column) for transverse velocities as a function of normalised separation distance r/δ_{th} for (a-f) cases A-F at $\bar{c} = 0.5$. Here, $D_{23,L}^{\alpha\beta*}(r)/(\tau S_L)^2$ and $D_{23,L}^{*}(r)/(\tau S_L)^2$ are normalised structure functions based on the density-weighted velocity $\vec{u}^* = \rho\vec{u}/\rho_0$.

Fig. 4: Variations of the probabilities for various events $P_{\alpha\beta}$ as a function of normalised separation distance r/δ_{th} for (a-f) cases A-F at $\bar{c} = 0.5$.

Fig. 5: Variations of normalised turbulent kinetic energy $\tilde{k}/S_L^2$ with $\bar{c}$ for (a-f) cases A-F.

Fig. 6: Minimal and maximal values of the transverse components of the unit normal vector $\vec{N} = -\nabla c/|\nabla c|$ found for each transverse plane corresponding to $\bar{c}$ =constant for (a-f) cases A-F.

Fig. 7: Maximal (over each transverse plane at $\bar{c}$) values of $|\vec{N} \cdot \nabla u_1|\delta_{th}/\tau S_L$ for $|N_2| \geq N^*$ and/or $|N_3| \geq N^*$ for different threshold values of N^*, as specified in legends, for (a-f) cases A-F.

Fig. 8: PDFs of $\left|\vec{N}\cdot\nabla u_1\right|\delta_{th}/\tau S_L$ for either $|N_2|\geq 0.95$ or $|N_3|\geq 0.95$ for different values of $\bar{c}$ for (a-f) cases A-F.

Fig. 9: Variations of $D_{23L,rr}/k_R$ with r/δ_{th} for different values of $\bar{c}$ for (a-f) cases A-F.

Fig. 10: Variations of the magnitude of the structure function $D_{23L,rr}$ normalised by its value for $\bar{c}=0.01$ (i.e. $D_{23L,rr}(r)/D_{23L,rr}(r;\ \bar{c}=0.01)$ for (a-f) cases A-F.

Fig. 11: Probability of finding the entire segment [A; B] within heat release zones ($0.75\leq c\ \leq 0.95$) for different values of $\bar{c}$ for (a-f) cases A-F.

Fig. 12: Variations of the normalised transverse structure functions $D_{11,hh}/\overline{u_1'^2}$ and $2D_{23,hh}/\{\overline{u_2'^2}+\overline{u_3'^2}\}$ as a function of the normalised r/δ_{th} for (a-f) cases A-F for different values of $\bar{c}$.

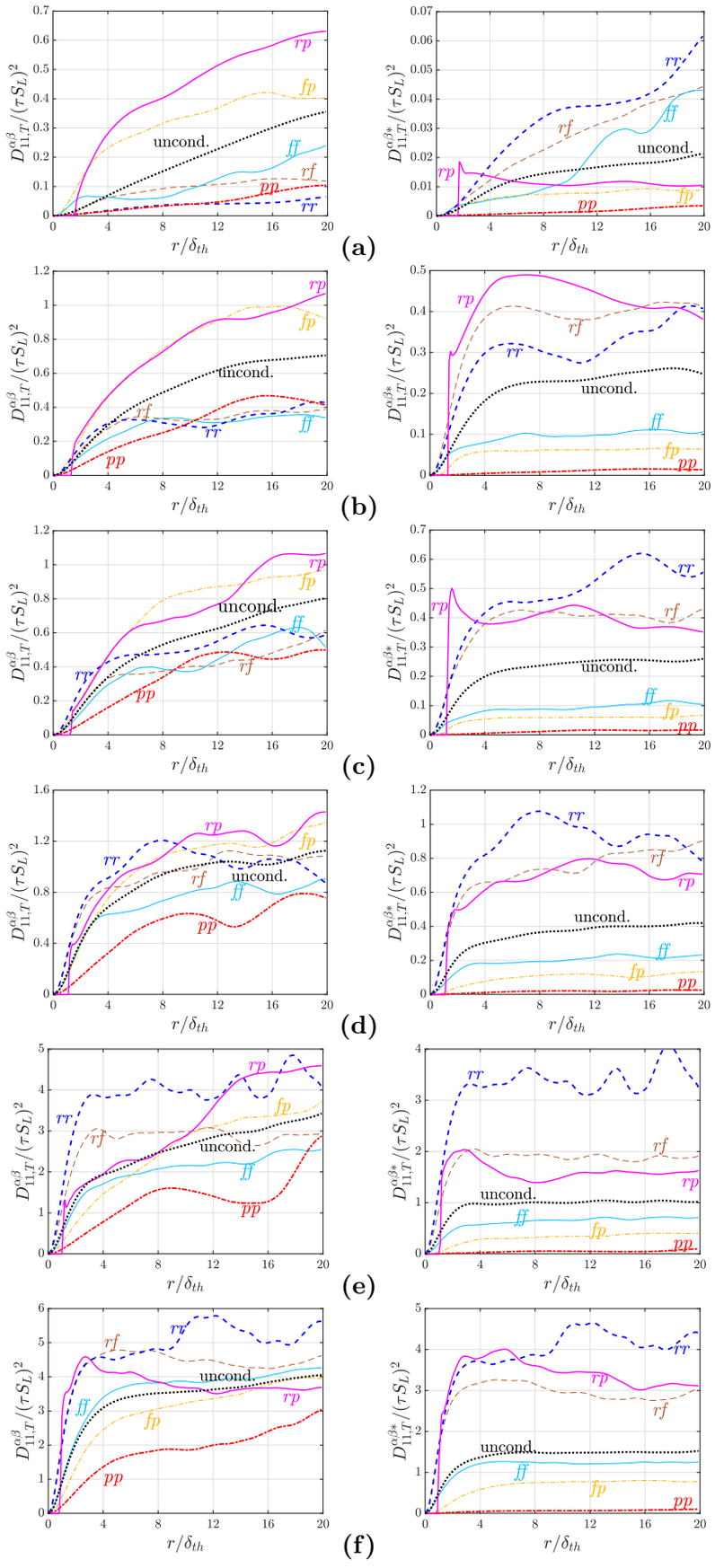

Fig. 1: Variations of normalised transverse conditioned structure functions (coloured lines) $D^{\alpha\beta}_{11,T}/(\tau S_L)^2$ (left column) and $D^{\alpha\beta*}_{11,T}/(\tau S_L)^2$ (right column) and mean unconditioned structure functions (black dots) $D_{11,T}/(\tau S_L)^2$ (left column) and $D^{*}_{11,T}/(\tau S_L)^2$ (right column) for axial velocities as a function of normalised separation distance r/δ_{th} for (a–f) cases A–F. Here, $D^{\alpha\beta*}_{11,T}/(\tau S_L)^2$ and $D^{*}_{11,T}/(\tau S_L)^2$ are normalised structure functions based on the density-weighted velocity $\vec{u}^* = \rho\vec{u}/\rho_0$.

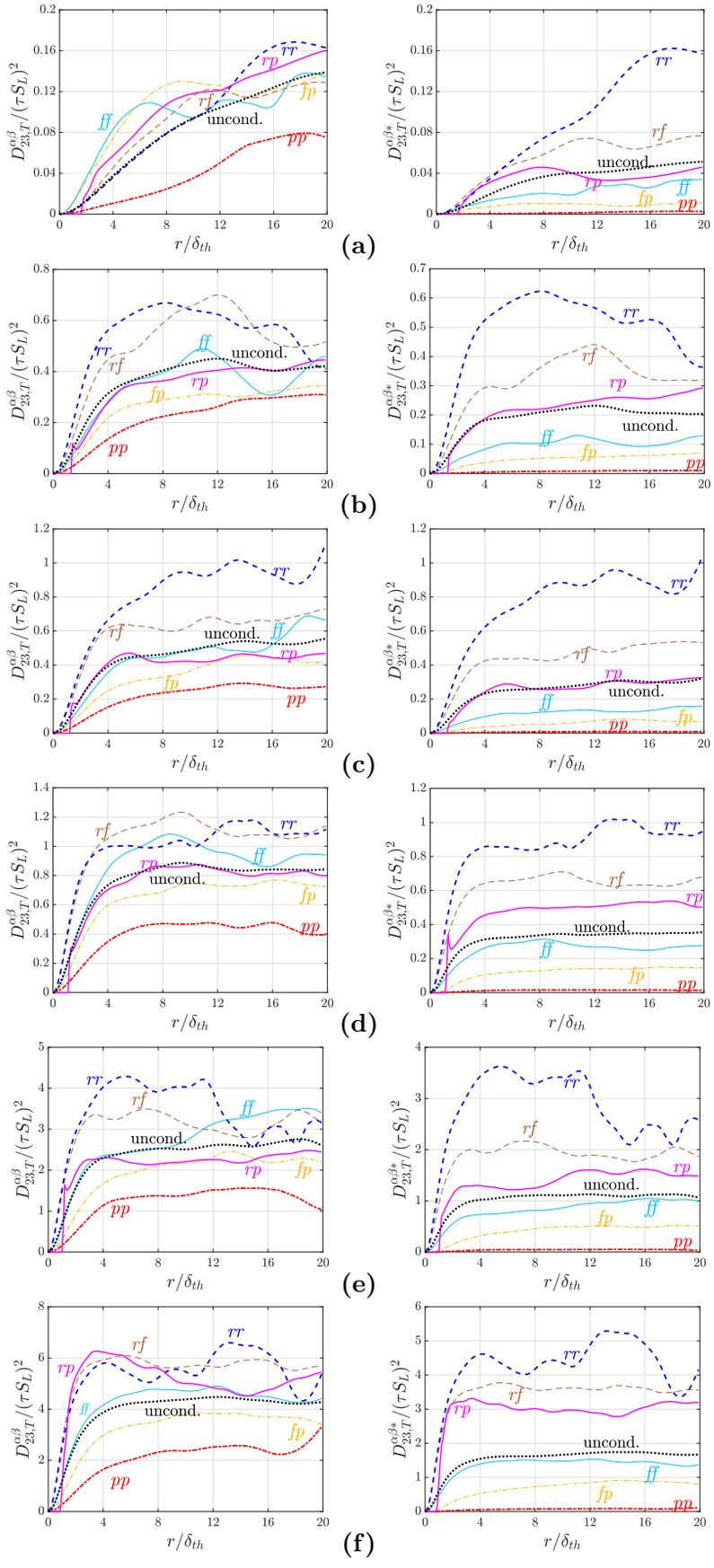

Fig. 2: Variations of normalised transverse conditioned structure functions (coloured lines) $D^{\alpha\beta}_{23,T}/(\tau S_L)^2$ (left column) and $D^{\alpha\beta*}_{23,T}/(\tau S_L)^2$ (right column) and mean unconditioned structure functions (black dots) $D_{23,T}/(\tau S_L)^2$ (left column) and $D^{*}_{23,T}/(\tau S_L)^2$ (right column) for transverse velocities as a function of normalised separation distance r/δ_{th} for (a–f) cases A–F. Here, $D^{\alpha\beta*}_{23,T}/(\tau S_L)^2$ and $D^{*}_{23,T}/(\tau S_L)^2$ are normalised structure functions based on the density-weighted velocity $\vec{u}^* = \rho\vec{u}/\rho_0$.

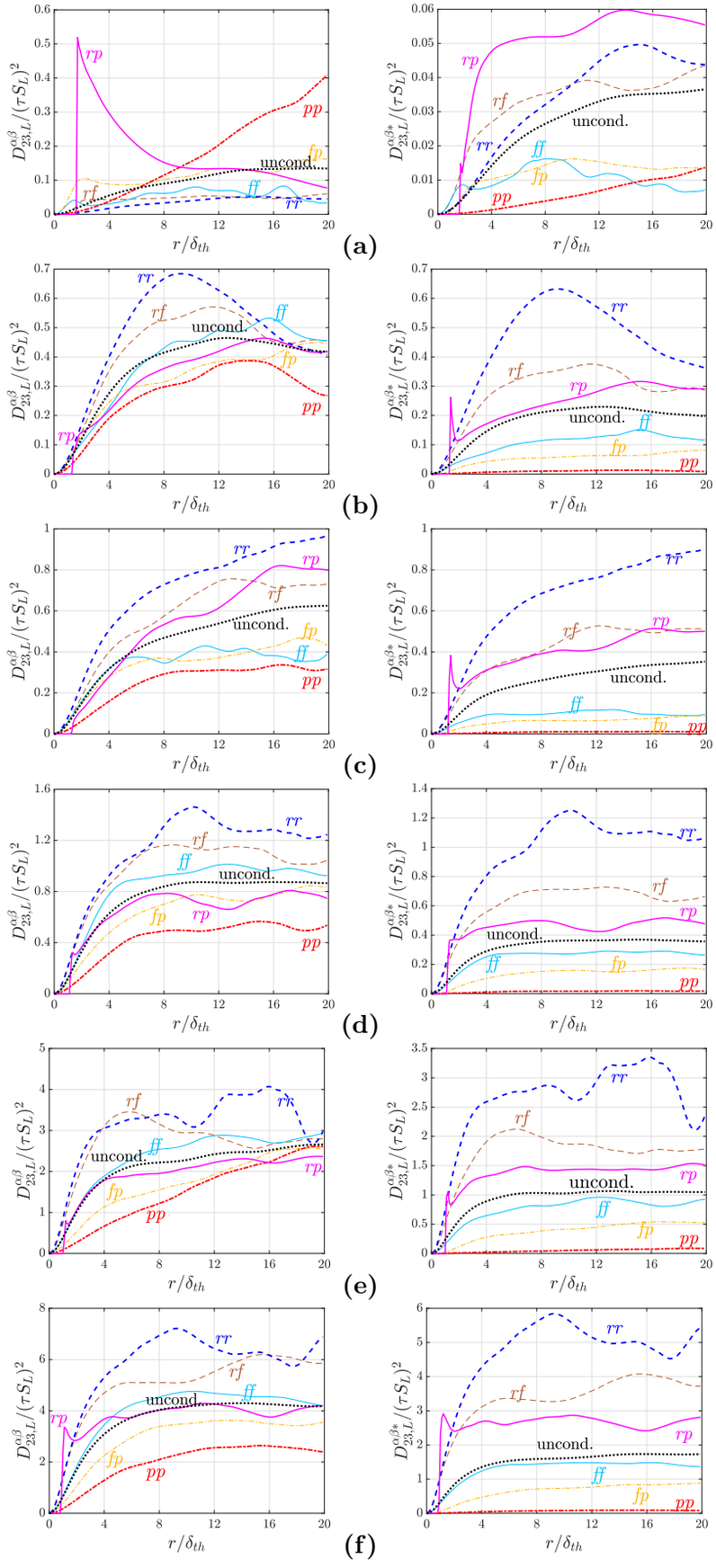

Fig. 3: Variations of normalised longitudinal conditioned structure functions (coloured lines) $D^{\alpha\beta}_{23,L}/(\tau S_L)^2$ (left column) and $D^{\alpha\beta*}_{23,L}/(\tau S_L)^2$ (right column) and mean unconditioned structure functions (black dots) $D_{23,L}/(\tau S_L)^2$ (left column) and $D^{*}_{23,L}/(\tau S_L)^2$ (right column) for transverse velocities as a function of normalised separation distance r/δ_{th} for (a–f) cases A–F. Here, $D^{\alpha\beta*}_{23,L}/(\tau S_L)^2$ and $D^{*}_{23,L}/(\tau S_L)^2$ are normalised structure functions based on the density-weighted velocity $\vec{u}^* = \rho\vec{u}/\rho_0$.

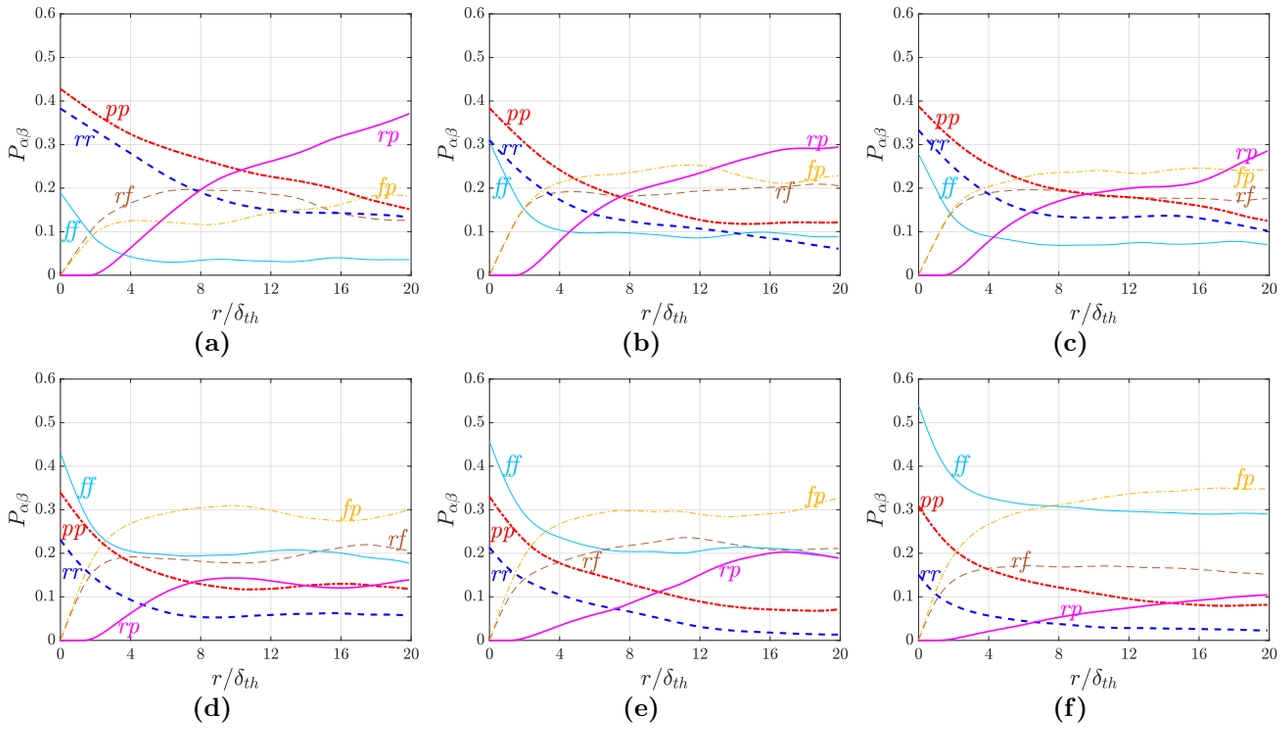

Fig. 4: Variations of the probabilities for various events $P_{\alpha\beta}$ as a function of normalised separation distance r/δ_{th} for (a–f) cases A–F at $\overline{c} = 0.5$.

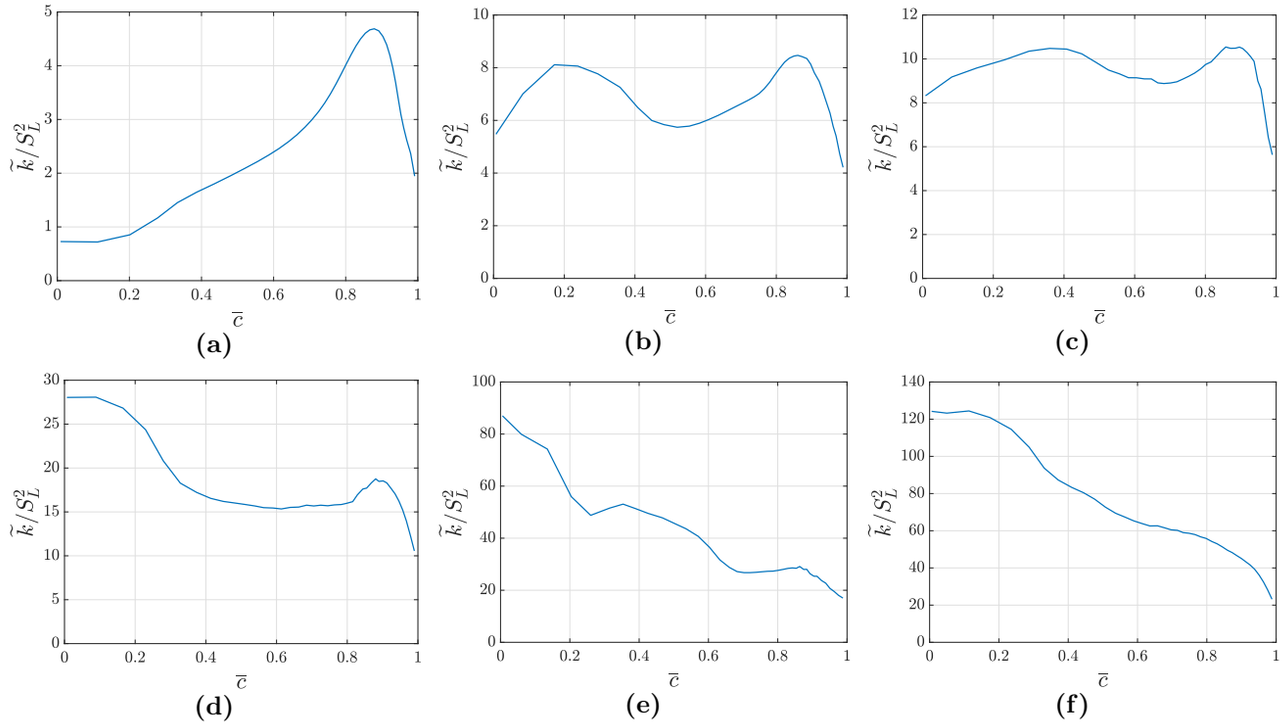

Fig. 5: Variations of normalised turbulent kinetic energy $\widetilde{k}/S_L^2$ with $\overline{c}$ for (a–f) cases A–F.

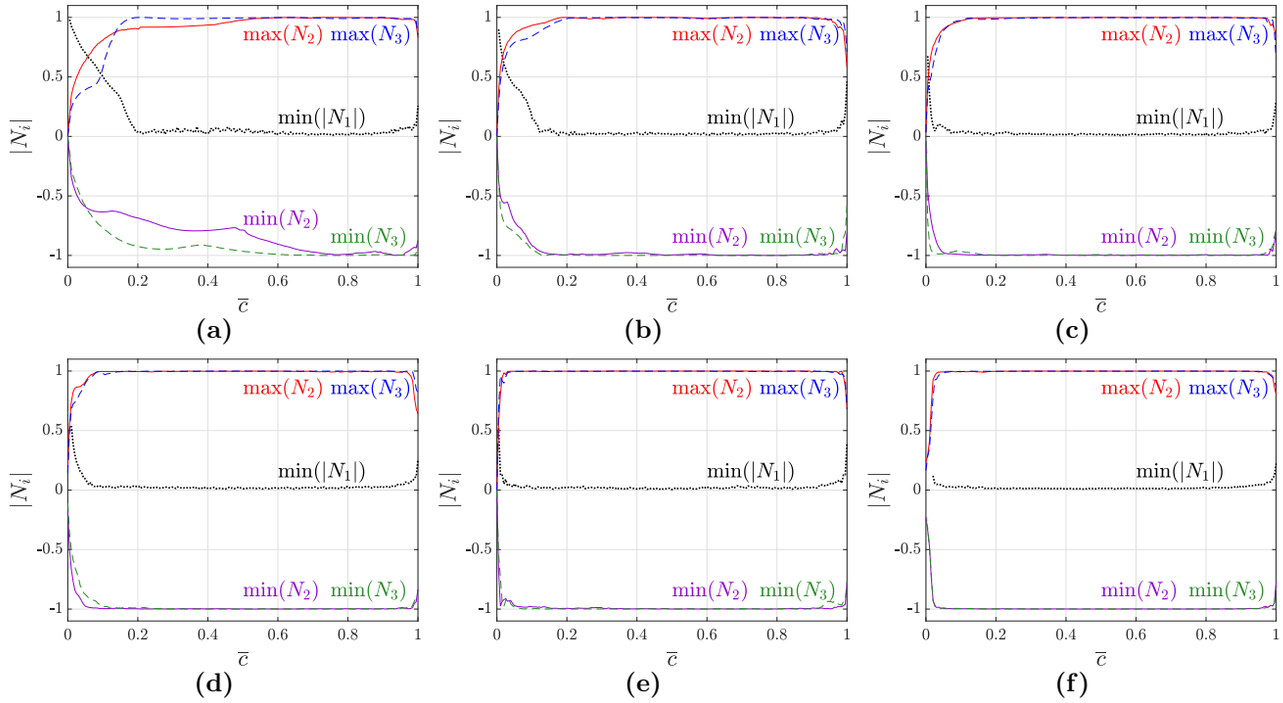

Fig. 6: Minimal and maximal values of the transverse components of the unit normal vector $\vec{N} = -\nabla c/|\nabla c|$ found for each transverse plane corresponding to $\overline{c}$ = constant for (a–f) cases A–F.

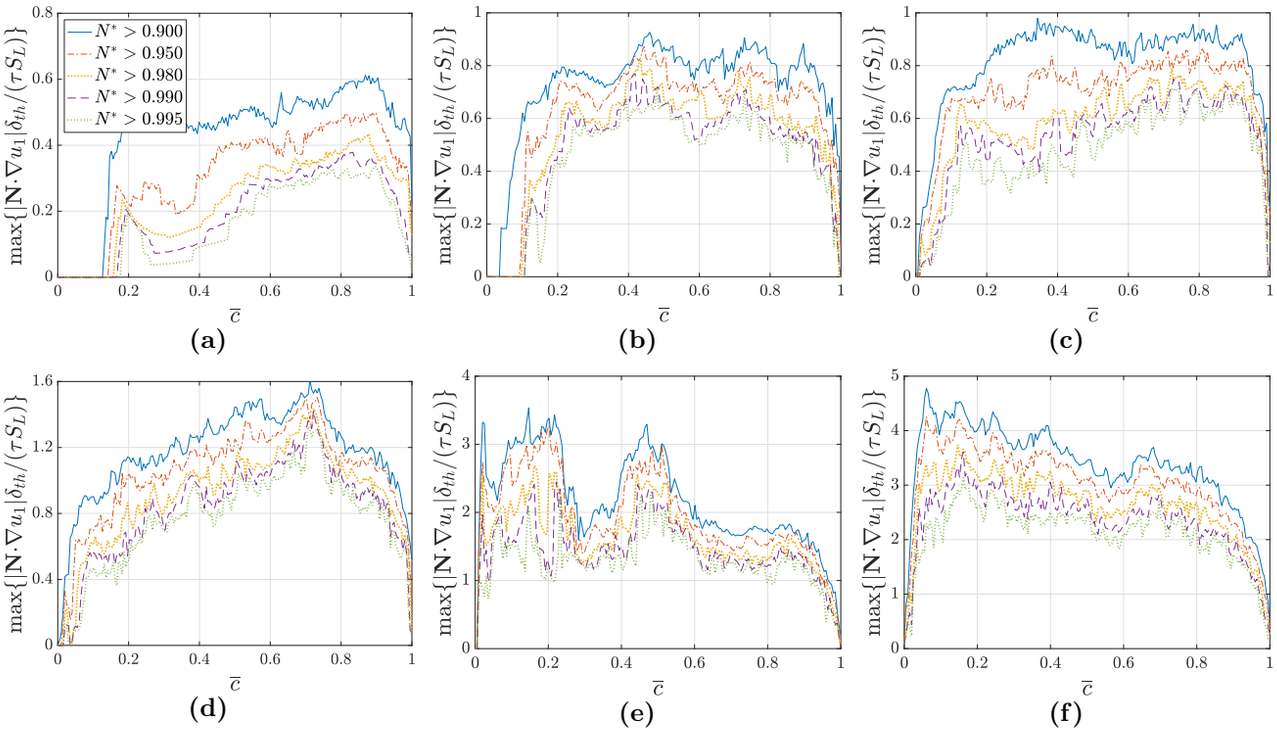

Fig. 7: Maximal (over each transverse plane at $\overline{c}$) values of $|\vec{N}\cdot\nabla u_1|\delta_{th}/\tau S_L$ for $|N_2| \geq N^*$ and/or $|N_3| \geq N^*$ for different threshold values of N^*, as specified in the legends, for (a–f) cases A–F.

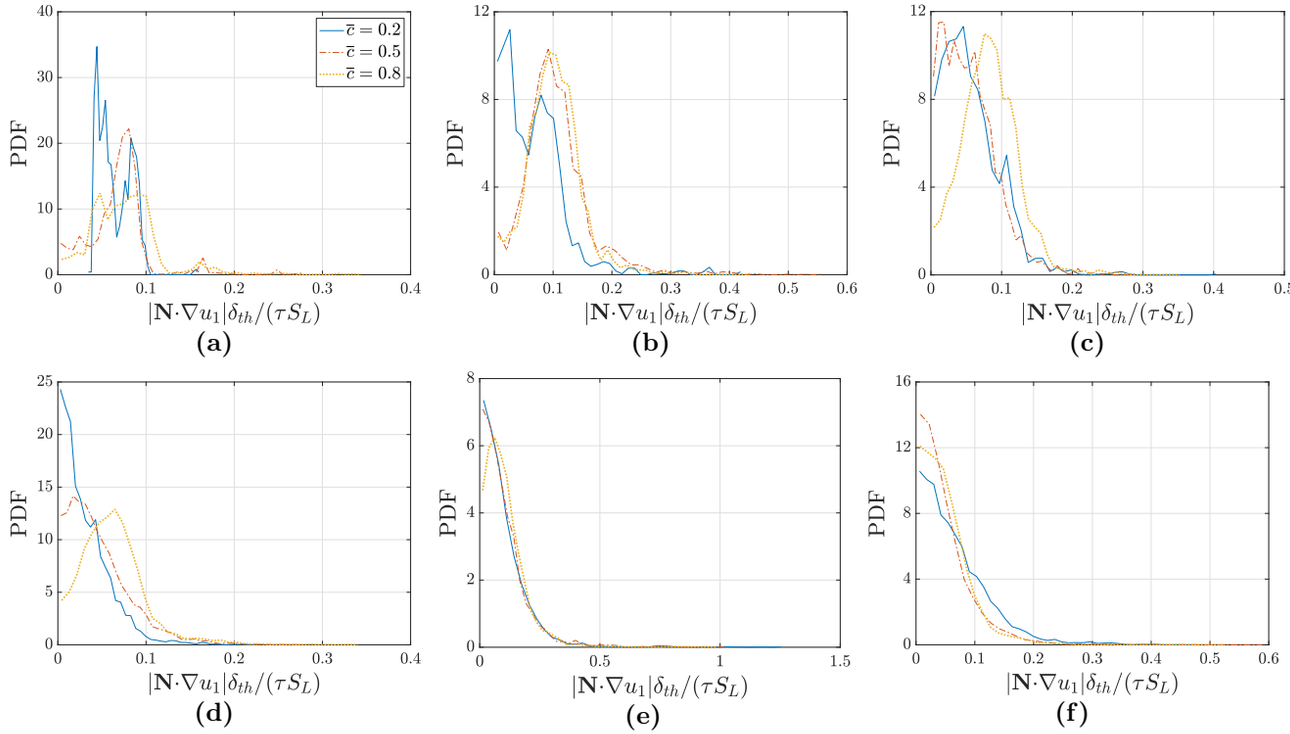

Fig. 8: PDFs of $|\vec{N}\cdot\nabla u_1|\delta_{th}/\tau S_L$ for either $|N_2| \geq 0.95$ or $|N_3| \geq 0.95$ for different values of $\overline{c}$ for (a–f) cases A–F.

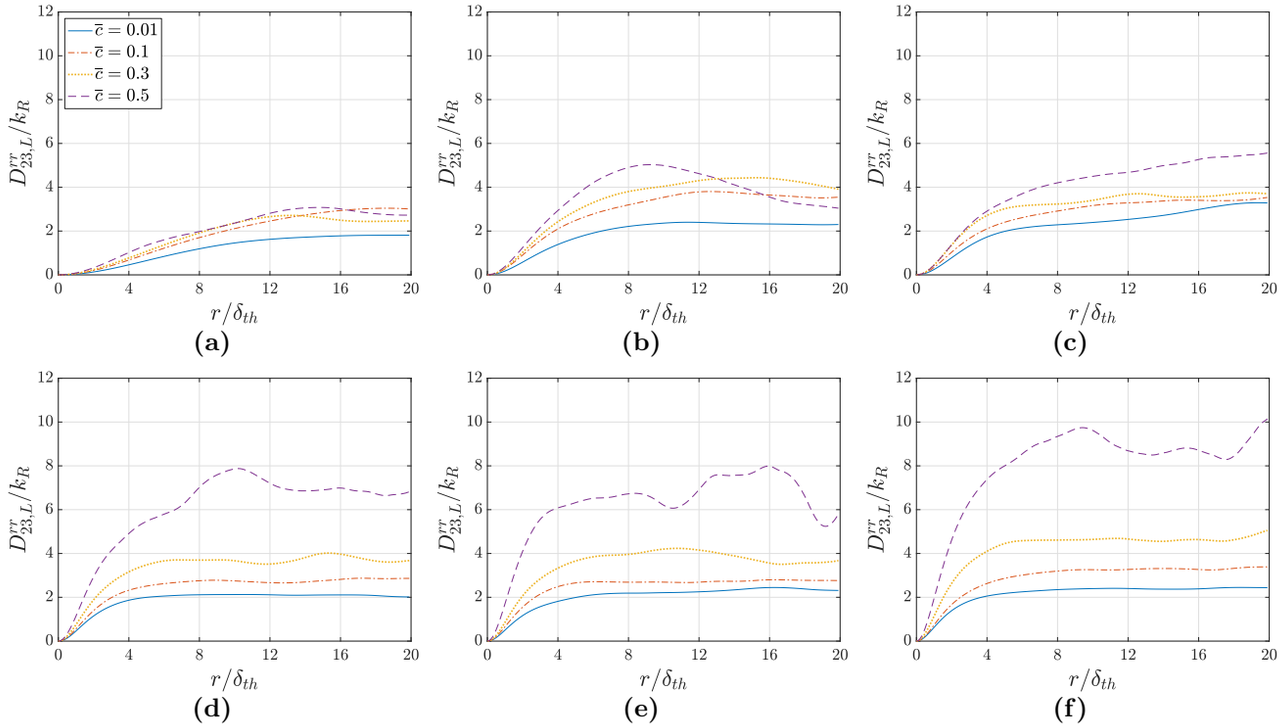

Fig. 9: Variations of $D^{rr}_{23,L}/k_R$ with r/δ_{th} for different values of $\overline{c}$ for (a–f) cases A–F.

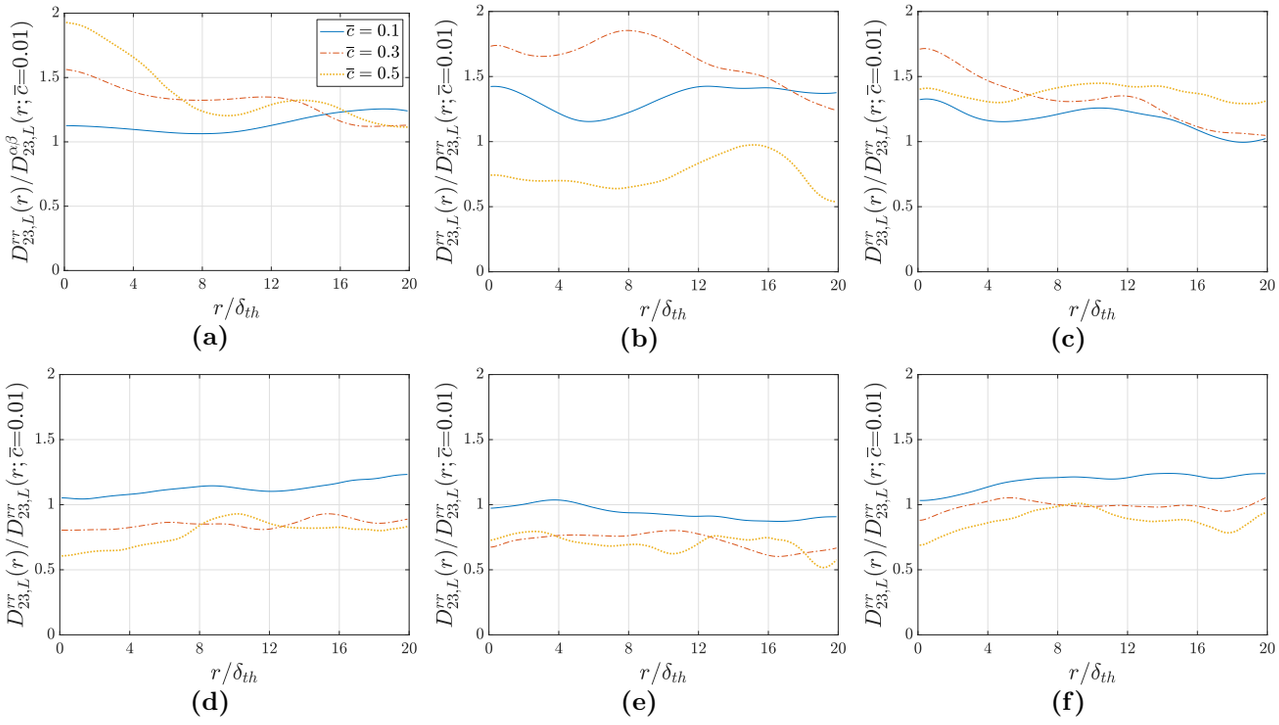

Fig. 10: Variations of the magnitude of the structure function $D^{rr}_{23,L}$ normalised by its value for $\overline{c} = 0.01$ (i.e. $D^{rr}_{23,L}(r)/D^{rr}_{23,L}(r;\overline{c} = 0.01)$) for (a–f) cases A–F.

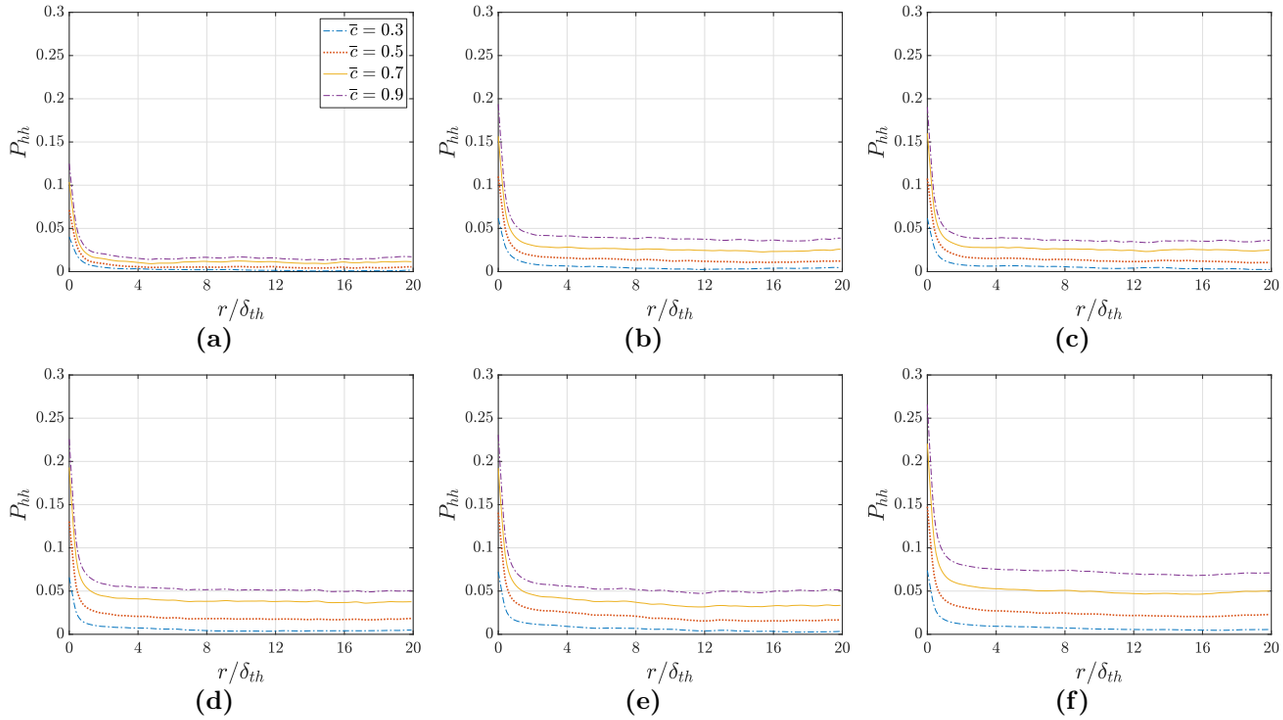

Fig. 11: Probability of finding the entire segment [A; B] within heat releasing zones ($0.75 \leq \overline{c} \leq 0.95$) for different values of $\overline{c}$ for (a–f) cases A–F.

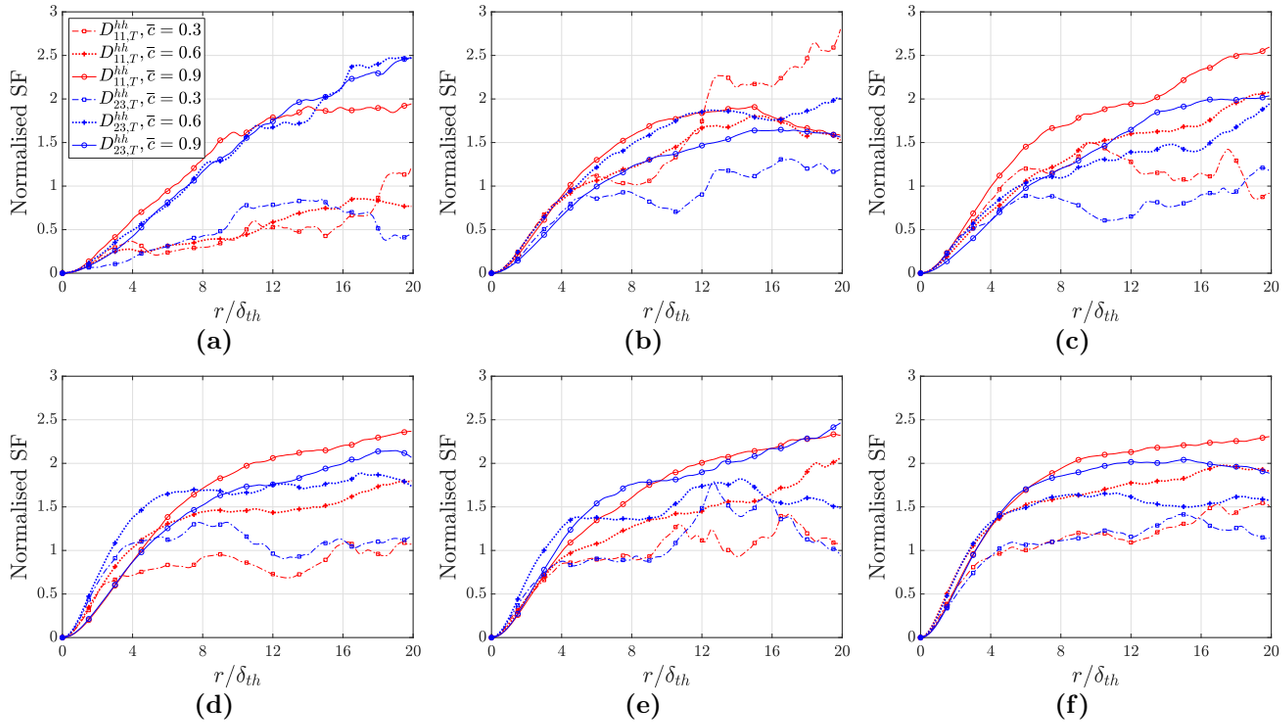

Fig. 12: Variations of the normalised transverse structure functions $D^{hh}_{11,T}/\overline{u_1'^2}$ and $2D^{hh}_{23,T}/\{\overline{u_2'^2} + \overline{u_3'^2}\}$ as a function of the normalised r/δ_{th} for (a–f) cases A–F for different values of $\overline{c}$.